Energy & Environmental Science

ROYAL SOCIETY OF CHEMISTRY

ANALYSIS

View Article Online
View Journal | View Issue

CrossMark click for updates

Cite this: *Energy Environ. Sci.*, 2016, **9**, 820

Deciphering the true life cycle environmental impacts and costs of the mega-scale shale gas-to-olefins projects in the United States†

Chang He‡ and Fengqi You*

Received 31st July 2015,
Accepted 16th February 2016

DOI: 10.1039/c5ee02365c

www.rsc.org/ees

This paper addresses the techno-economic-environmental analysis of large-scale olefin production from shale gas in the major shale regions of the U.S. (including Appalachian, Gulf Coast, Mid-Continent, and Rocky Mountain regions) and investigates its environmental footprints. To decipher the true production costs and environmental impacts, we first develop shale gas supply and olefin production network models to estimate pipeline distances, numbers of wells, well-sites, and gathering systems needed in the near- and mid-term. Next, detailed process design, modeling, and integration methods for alternative technologies are developed. We conduct life cycle analysis (LCA) to systematically evaluate the energy–water–carbon nexus. Based on the economic and LCA results, we compare the influences of gas composition, project operating time, well lifetime, and the allocation method. The results indicate that the four shale regions considered would in total supply feedstocks for U.S. ethylene production for at least 130 years. However, only olefins produced from Gulf Coast and Mid-Continent regions demonstrate economic advantage ($668 per t and $255 per t) over ethylene in the current market. Based on the mass-based allocation approach, for the four shale regions evaluated, the energy consumption is 13.8–17.2, 14.3–16.7, 13.3–16.7, and 12.2–14.5 GJ per t olefins, and the freshwater footprint is 3.31–4.28, 5.34–5.65, 3.05–3.56, and 4.68–5.03 kg kg^{-1} olefins, respectively. In addition, normalized GHG emissions indicate that shale gas can be categorized as a low-carbon feedstock (0.75–1.05 kg CO_2-eq per kg) based on a mass-based allocation approach, or a high-carbon feedstock (1.24–2.13 kg CO_2-eq per kg) based on an economic value-based allocation approach.

Broader context

With focus on the shale gas-to-olefin (STO) project, systematic studies on process design, techno-economic modeling, and environmental impacts have captured growing attention. This work addresses the techno-economic-environmental analysis of large-scale STO projects in the U.S. and investigates the production cost and the energy–water–carbon nexus in the near/mid-term. The results indicate that all shale regions would in total provide at least 130 years' worth of feedstock supply, but current economic climate renders the STO approach prohibitive. Besides, following a mass-based allocation method, STO could be an attractive approach with relatively mild environmental impacts. However, this optimistic viewpoint would be completely altered if we employ an economic value-based allocation method in which the shale gas has a greater carbon footprint than naphtha. Furthermore, we identify that the well lifetime is the most critical factor that significantly influences the environmental impacts of the STO project.

1. Introduction

U.S. natural gas (NG) production rapidly increases due to increasing exploitation of shale rocks, reshaping the domestic energy landscape for decades to come. This trend potentially affects not only the fuel market but also the entire petrochemical industry since most of the shale gas resources in the U.S. are reported to be fairly rich in natural gas liquids (NGLs).[1,2] Between 2008 and 2014, NGL production from gas processing facilities increased by 61.1% from 1.80 to 2.90 million barrels per day.[3] In particular, both ethane and propane fractionated from the NGLs are important feedstocks for production of olefins, which significantly benefit the downstream petrochemical industry.[1,4] This has allowed the U.S. petrochemical industry to take a competitive global position in chemical production.[3] Based on a Platts analysis,

Department of Chemical and Biological Engineering, Northwestern University, Evanston, IL 60208, USA. E-mail: you@northwestern.edu; Fax: +1 (847) 491-3728; Tel: +1 (847) 467-2943

† Electronic supplementary information (ESI) available. See DOI: 10.1039/c5ee02365c

‡ Current address: School of Chemistry and Chemical Engineering, Key Lab of Low-carbon Chemistry & Energy Conservation of Guangdong Province, Sun Yat-Sen University, No. 135, Xingang West Road, Guangzhou, 510275, China.

new shale gas-to-olefin (STO) projects would boost U.S. ethylene production by at least 8 Mt (megaton) per year.[5] However, a thorough success of shale gas projects is still far from proven at the current stage, as multiple concerns regarding economic competitiveness and environmental impacts should be addressed.

Shale gas producers in the U.S. are in a pessimistic economic climate. Recent statistical reports show that most shale wells had a lifetime far less than expected (even <10 years), leading to a low estimated ultimate recovery (EUR).[6–8] The low EUR raises the production cost to higher than \$4 per MMbtu, making the shale gas production in the U.S. unprofitable under the current NG prices due to the collapse in oil prices.[9] The low oil prices also drag olefin price down, so STO projects in the U.S. are currently uncompetitive. Besides, the shortage of infrastructure including processing facilities and gathering systems further exacerbates the economic competitiveness of shale gas projects. Deciphering the real production cost of olefins from shale gas involves the simultaneous consideration of plant-level production costs,[10,11] feedstock costs, and transportation costs.

Environmental impacts of shale gas projects are of particular interest. In the upstream gas production stage, shale gas production is reported to consume 1.4–3.9 times more freshwater than conventional NG production over its life cycle.[12,13] Accordingly, there are several publications addressing the design and operations of water supply chains in shale gas production.[14–18] Unlike freshwater withdrawal, GHG emissions (especially methane fugitive) during well drilling and completion are more difficult to measure. A variety of LCA studies have examined the carbon footprints of shale gas production, but the conclusions in these studies are contradictory regarding whether shale gas is a low carbon fuel or not.[19–22] In addition to upstream shale gas production stages, there are environmental concerns on carbon conversion involved in downstream gas processing and olefin production, because a considerable amount of refrigerant, electricity, fuel, and freshwater is consumed. Therefore, systematic LCA studies on the energy–water–carbon nexus that cover the entire life cycle of olefins are needed to determine the actual environmental footprints. However, to the best of our knowledge, no existing studies apply life cycle thinking and tools to the STO projects.

More specifically, it is worth emphasizing that some practical issues potentially influencing project performance should be taken into account. The first is the location of the STO projects. It is generally acknowledged that the shale regions (or plays) being developed in the U.S., as shown in Fig. 1, do not constitute homogenous resources.[24] Each region has its own set of particular geological, geo-chemical, and petrophysical characteristics, so the average gas EUR, lifetime, well spacing, gas composition, energy and water consumption, GHG emissions, and the construction cost of a single well can vary between regions. The above properties can ultimately alter one location's favorability over another. The second issue is how the integrated shale gas projects are operated and maintained over their lifetime. From the standpoint of feedstock supply, a mega-scale cracking plant would involve thousands of wells, tens of processing facilities, and hundreds of miles of transportation pipelines. Thus, unlike previous studies on NG (ethane)-to-olefins,[25,26] the overall performances of shale gas projects are more susceptible to the numbers of wet wells (wells that have NGL production) and processing facilities. Of particular attention is the project

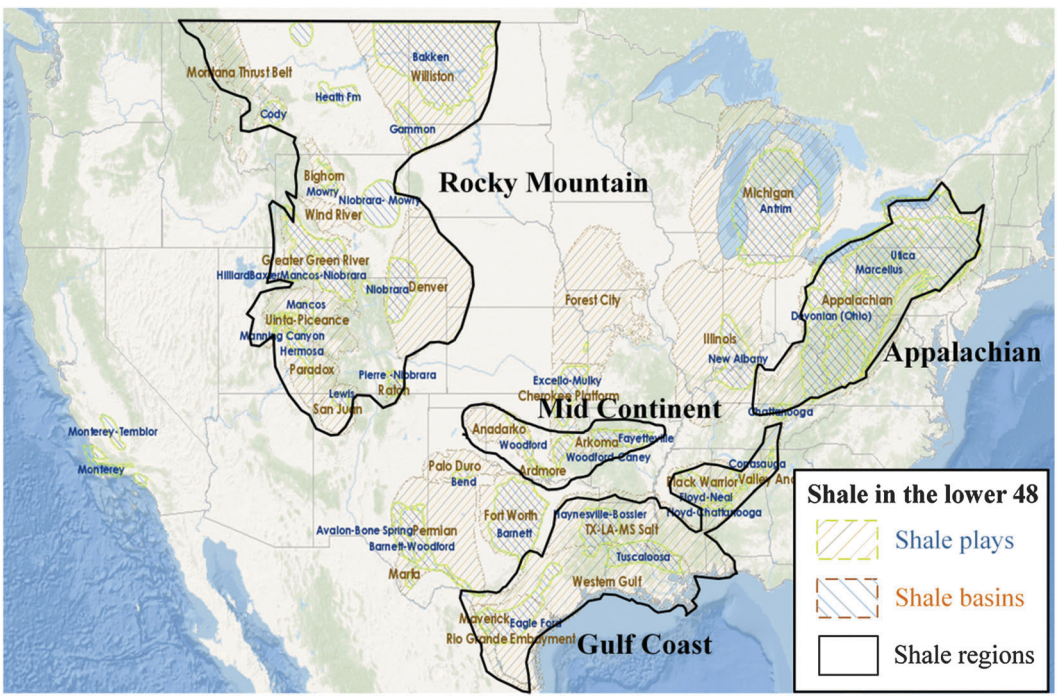

Fig. 1 Appalachian, Gulf Coast, Mid-Continent, and Rocky Mountain Shale regions evaluated in this study (updated from the ArcGIS database[23]). The detailed information (play name, well number, area, *etc.*) related to this figure is provided in Table S1 in ESI† and Table 1.

operating time that would indirectly affect the absolute environmental footprints in shale gas production, as more wet wells are required as time goes by. Furthermore, the overall process is a very complex carbon conversion network that includes nearly half a dozen reactors, a dozen compressors, and two dozen separators. Accurate process simulation and efficient utility integration are necessary to assess the plant-level energy losses, freshwater withdrawal, and CO_2 leakage.

This work systematically addresses the techno-economic-environmental analysis of mega-scale STO projects in the U.S., and investigates the production cost and the energy–water–carbon nexus in the near- and mid-term. These STO projects involve 439 454 wet shale wells (wells with the NGL output) located in four main shale regions including Appalachian, Gulf Coast, Mid-Continent, and Rocky Mountain, as illustrated in Fig. 1. To decipher the real production cost and environmental impacts, we first introduce detailed feedstock supply and olefin production network models which cover the complete process from shale wells to petrochemical facilities. Specifically, a distributed-centralized STO model is used to quantitatively estimate the numbers of shale wells, well-sites, and gathering systems, as well as distances of gathering pipelines required for the mega-scale olefin production in the four shale regions. In addition, we investigate the influences of project operating time (near- or mid-term) on the analysis results due to the production profile of a shale well. Next, in order to determine mass and energy balances, we present rigorous process design and simulation models for the candidate technologies and options, as well as integration methodologies to minimize both energy and fresh water usage. Based on the above studies, we conduct a comprehensive investigation of the energy–water–carbon nexus by determining life cycle energy consumption, life cycle freshwater footprints, and life cycle GHG emissions. Last, the influences of project operating time, well lifetime, the allocation method, and feedstock composition are compared and discussed.

2. Supply and production models

2.1 Distributed-centralized model

In a conventional process, the raw shale gas extracted from a wellhead is first gathered at a nearby well-site (see Fig. 2(a)) where most flowback water and associated oil are rejected. Depending on the wetness of the raw shale gas, the gas producer can directly process this gas, or sell it to midstream companies by gathering pipelines. Fig. 2(b) depicts how the gathered gas is further purified and compressed by a processing facility, resulting in processed gas that satisfies pipeline specifications for the heating value, impurity content, and pressure. Marketable NGLs separated from the pipeline gas are fractionated, stored, and then transported in a variety of forms like Y-grade stream, E–P mix and LPG stream.[3] For long-distance transportation of NGLs, pipeline transportation is a superior mode compared to rail or highway due to its low unit cost and higher capacity. Finally, NGLs purchased from midstream market hubs/centers can be used as feedstocks in the downstream petrochemical processes to produce a number of value-added chemicals.

In a new STO process, the petrochemical plant is co-located with shale plays and gas processing facilities. The raw shale gas is processed in multisite distributed processing facilities, and then the recovered NGLs are moved to a centralized steam cracking plant where the NGLs are fractionated and pyrolyzed. The distributed processing facility is considered at four scales: 50, 100, 200, and 300 MMscfd of raw shale gas input. To estimate the transportation distance, we consider the distributed processing facilities located in a hypothetical square area, as shown in Fig. 2(c). In particular, a total of 594 922 shale wells from the EIA report[28] are assumed to be evenly distributed in both developed and undeveloped areas of each shale region. In this model, only 439 454 wet wells are considered using the ratios of dry wells to wet wells mainly sampled by Zavala-Araiza *et al.*,[27] see Fig. 3(a and b) and Table S2 in ESI.† This consideration is made because the dry well generally has no NGL output and has no impact on olefin production, the techno-economic results or the LCA results from the system boundary. Furthermore, the average well area given in Fig. 2(c) and Table S1 in ESI,† together with processing capacity and other coefficients (*i.e.*, terrain factor), are used in the estimation of gas/oil production and transportation distances (see Section 1.3 in ESI†).

2.2 Near/mid-term shale gas production

As mentioned above, two time periods, namely near-term (0–5 year) and mid-term (6–10 year), are considered in shale gas production as shown in Fig. 3. Compared with near-term production, the mid-term production needs additional NGL supply from new wet wells to maintain the same plant size due to the declining production profiles of shale wells. As shown in Fig. 4, when a shale well begins production, it has a short period of preproduction (about 1 month, but this period can be ignored in most cases). Its production rate, $P(t)$, will increase up to a peak ($t = t_0$), followed by a significant decrease ($t > t_0$), which exhibits a hyperbolic decline curve. Note that the yield of a well at the end of the first year usually decreases to 10–20% of the production peak. This translates into production of 15–40% of a well's EUR within the first year. After that, the production decline slows through the next five years until the daily rate stabilizes in the seventh or eighth year where it tends to remain fairly constant. This trend clearly illustrates the significant decline in the cumulative production for a well in the mid-term compared to that of a well in the near-term. The cumulative production for a well is estimated using the decline curve analyses (DCA) and historical production data. More specifically, this work uses a classical Arps empirical[27,29] decline formula (shown in Fig. 4) to generate a forecast of future production.

$$q = \int_{t_1}^{t_2} P(t)\mathrm{d}t \approx P_{t_1} \times \int_{t_1}^{t_2} 1/(1 + b \times D \times t)^{1/b}\mathrm{d}t \qquad (1)$$

where P_{t_1} is the initial production rate at time t_1; D and b are the initial decline rate and the decline exponent which can be determined from the regression of historical data (see Tables S3–S6 in ESI†). Other parameters including a and $P^{\dagger}$ can be calculated

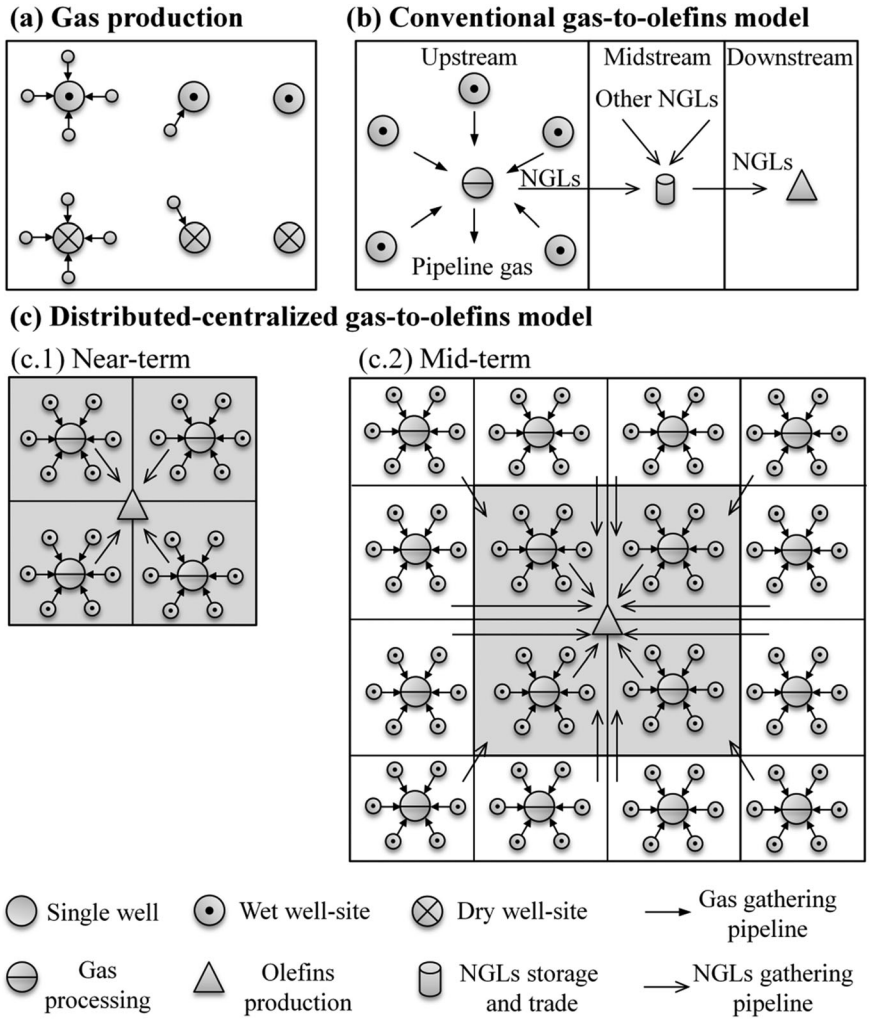

Fig. 2 Simplified shale gas supply and olefin production network models. (a) A well-site usually has multiple wells, single well, and sometimes no well,[27] this model assumes a well-site containing four wells on average; (b) the conventional STO process includes upstream, midstream, and downstream steps; (c) the proposed distributed-centralized model contains multisite distributed processing facilities and a centralized olefin production plant.

using a linear equation, $P(t) = a \times t + P^{\dagger}$, as shown in Fig. 3, and production data listed in Tables S3–S6 in ESI.† The results of decline parameters (a, b, $P^{\dagger}$, and D), near/mid-term production (NT/MT), and EUR estimated for 20 or 10 year well lifetime (20/10 year EUR) are summarized in Table 1. Note that the associated oil production can also be calculated *via* eqn (1).

2.3 Feedstock cost and properties

Another characteristic is the variation of composition of raw shale gas in the near-term and mid-term.[1] To mitigate this uncertainty, we estimate the average composition of impurity-free shale gas using the cumulative production from 51 wet well-sites (181 wet wells) listed in Tables S7 and S8 in ESI.† In addition, the representative concentrations of impurities (*e.g.*, acid gases and N_2, see Table S9 in ESI†) are added to the impurity-free gas, and the resulting normalized concentrations are given in Table 1.

In this study, we assume that the raw shale gas is directly purchased from a wellsite at its production cost. The production cost of raw shale gas is highly correlated to well construction (drilling and completion) investment and EUR, and thus varies from well to well. To estimate the real cost, a discounted cash flow model is used to calculate the break-even gas selling price (BGSP, $ per MMbtu). This model estimates the BGSP at which the shale gas producer can achieve an 8% internal rate of return (IRR), using a full-cycle per-well approach.[30,31] Note that the revenue from the co-produced oil that can improve the project economics has been taken into the calculation of BGSP.

3. Plant modeling and integration

3.1 Process design and simulation

As indicated by the flowsheet diagram of the distributed-centralized STO model outlined in Fig. 5, producing olefins from shale gas proceeds through two conversion stages for which several candidate technologies and options are explored. In the first stage, each processing facility includes six processing units: gas sweetening, sulfur recovery, dehydration, NGL recovery, N_2 rejection,

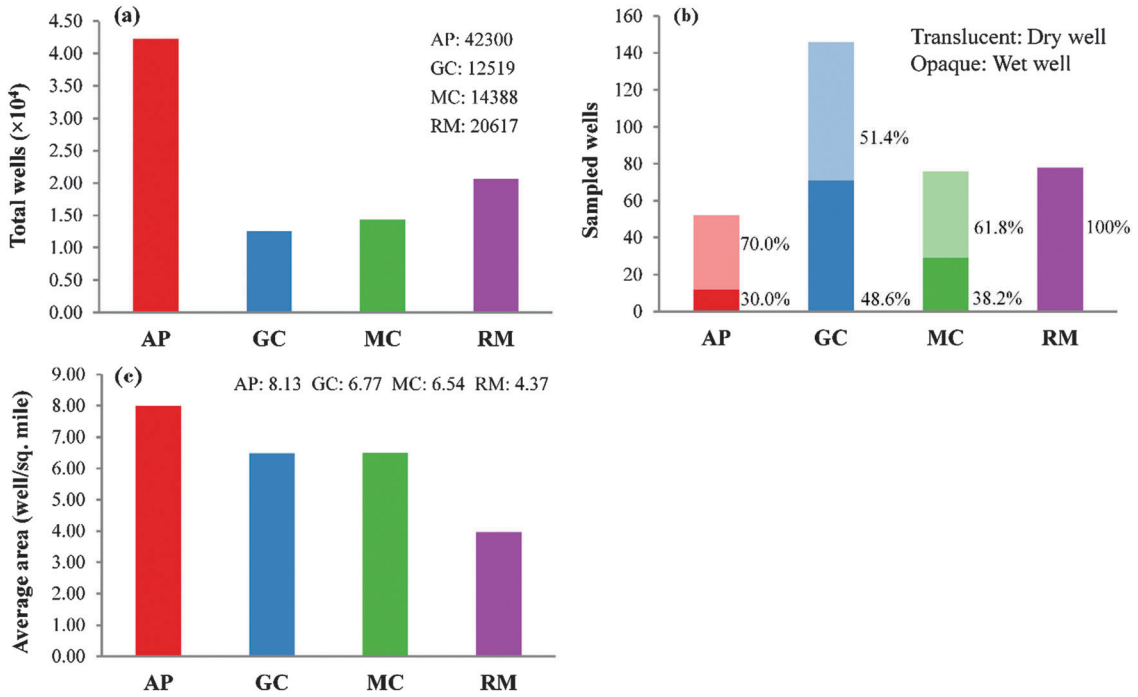

Fig. 3 Total shale wells, fractions of wet wells and dry wells, average area, and ages in Appalachian (AP), Gulf Coast (GC), Mid-Continent (MC), and Rocky Mountain (RM) regions. More details are provided in Tables S1 and S2 in ESI.†

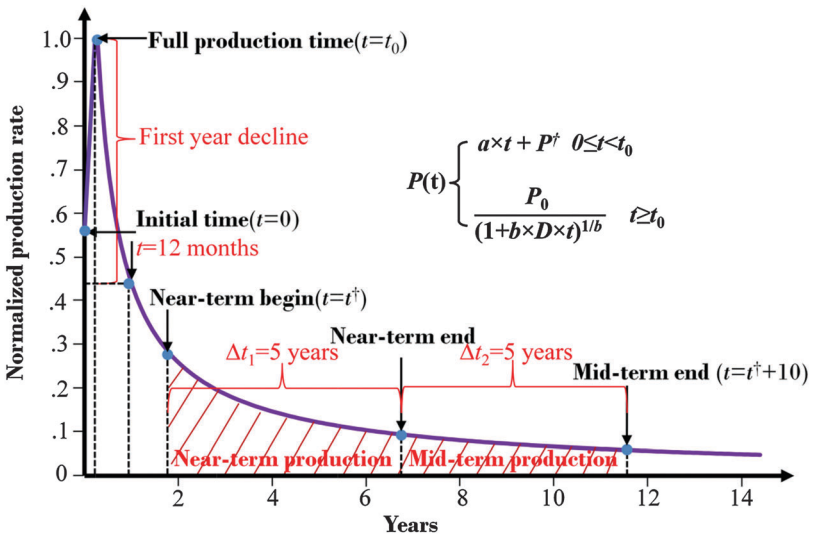

Fig. 4 Shale gas production decline rate curve.

and a compression station.[10,11] For the next stage, NGLs produced from multisite processing facilities are moved to a centralized plant including NGLs fractionation, mixture cracking, olefins separation, and utilities facility units. The utility facility can handle combined heat and mass streams from all possible sources in the centralized plant, in order to minimize the consumption of the required utilities including steam, refrigerants, water, and fuel. The cracking furnace could be fired with fuel gas, a waste by-product from the subsequent olefin separation unit or purchased from the external market. The general assumptions and default operating conditions used in process simulation are summarized in Table S13 in ESI.† The process description is provided in detail as follows.

3.1.1 Distributed shale gas processing facility. In order to prevent the equipment and pipeline from being corrupted, H_2S concentration should not exceed 4 ppm.[33] In addition, CO_2 concentration in the feed gas of the NGL recovery unit should fall between 0.01 mol% and 2.00 mol% to avoid potential freezing problems.[33] H_2S content in most of the shale gases is reported to vary typically within a very low molar range of H_2S

Table 1 Estimated raw shale gas properties (wt%), production parameters, and cost. Calculation details are given in the ESI

Region	C_1	C_2	C_3	C_4	C_5	CO_2	H_2S[a]	N_2	H_2O[b]	HHV btu per scf	Decline parameters ($a/b/P^*/D$)	Gas q, bcf (NT/MT)	Gas EUR, bcf (20/10 year)	Oil q, MBO[c] (NT/MT)	Oil EUR, MBO (20/10 year)
Properties and production parameters															
AP	80.99	8.56	2.30	0.96	0.54	1.80	0.74	2.54	0.10	1035	0.655/1.5090/0.345/0.2540	0.51/0.20	0.97/0.71	0.18/0.07	0.35/0.26
GC	50.81	16.13	9.57	6.39	5.14	9.27	2.44	0.15	0.10	1215	0.528/1.2065/0.472/0.2522	2.11/0.64	3.49/2.75	9.75/2.97	16.1/12.7
MC	71.40	11.31	7.13	3.33	2.53	2.44	0.62	1.15	0.10	1133	0.544/1.1265/0.456/0.1022	1.19/0.43	2.16/1.62	34.2/12.4	61.1/46.6
RM	50.22	16.77	11.27	7.17	6.63	1.10	0.29	6.45	0.10	1256	0.470/1.4438/0.530/0.2994	0.61/0.21	1.06/0.82	25.1/8.84	16.8/13.0

Region	Construction (MM$)[30–32]	Royalty[d] (MM$)	Land use[e] (MM$)	Expense[f] ($ per bbl)	Oil revenue ($ per bbl)[27]	Severance (%)	Discount rate (%)	BGSP[g] (20/10 year)
Full cycle cost evaluation								
AP	3.00	0.68	0.38	0.71	100	7.50	8.00	8.35/7.48
GC	8.50	1.91	0.49	0.71	100	7.50	8.00	4.79/4.33
MC	5.50	0.90	0.49	0.71	100	7.50	8.00	4.03/3.35
RM	5.00	1.01	0.56	0.71	100	7.50	8.00	7.09/6.03

[a] H_2S/CO_2 is assumed to be 0.33 on molar basis. [b] Water concentration is set to 0.10 wt%. [c] MBO stands for thousand barrels of oil. [d] Royalty rate = 22.5% of construction cost.[30] [e] Land cost is 3.2 MM$ per sq. mile (5000 $ per acre).[30,31] [f] Expense is mainly related to operation and maintenance, $0.71 per MJ ($0.75 per MMbtu).[31] [g] All lease and capital costs occur in year 0, and production begins 0.5 year later.

to CO_2 (0.01–0.5).[34] Thus, a lower CO_2 content usually leads to a much lower H_2S content in the raw gas. To efficiently neutralize the raw gas, three technological alternatives are considered in the gas sweetening unit shown in Fig. 4 and 6a: (1) when the gas is only slightly sour, a fixed-bed type scavenger process would be a cost-effective approach for H_2S removal;[35] (2) a chemical absorption-based acid gas removal (AGR) process followed by a scavenger process works well for raw gas with moderate to high content of CO_2 and low content of H_2S; and (3) for moderate amounts of H_2S, sulfur must be captured by a sulfur recovery unit when its amount exceeds a limit specified by the environmental regulations, as suggested by Parks *et al.*[36]

In the last two hybrid processes, diethanolamine (DEA) is employed as a solvent in the AGR process because it can unselectively and effectively remove both H_2S and CO_2. The AGR process uses an "absorber + stripper" configuration in which acid gases are dissolved in the lean DEA by the absorber and are then released in the overhead gas by the stripper. However, the overhead gas contains low levels of H_2S (<40 mol%) and has a high CO_2/H_2S molar ratio (3.0–8.0), making it unsuitable for sulfur recovery directly using the Claus process.[36] An acid gas enrichment (AGE) process with methyl-diethanolamine (MDEA) is able to provide a higher H_2S content gas as shown in Fig. 6b; MDEA is a selective solvent, and the equilibrium solubility of H_2S in MDEA is much higher than that of CO_2.[37] The MDEA solvent preferentially absorbs H_2S and allows about 80% of the rejected CO_2 to remain in the CO_2 slip. Next, an AGE stripper can co-process the rich solvent drawn back from the SCOT absorber. After the AGE process, the enriched acid gas containing above 70 wt% H_2S is sent to a Claus section. To meet the stoichiometric requirements of the Claus reaction, a slight excess of air is added to oxidize 34.0% of H_2S to SO_2. The produced SO_2 then reacts with the oxidized H_2S in the bypassed acid gas to yield sulfur, a by-product. The Claus tail gas contains a small amount of H_2S (0.5–2.0 mol%), which can be removed *via* a shell Claus off-gas treating (SCOT) process. In the SCOT process, the tail gas is first heated to the reaction temperature before entering a catalytic hydrogenation reactor. The reactor effluent is condensed to 35 °C by sequentially passing through a heater and a quench column with spraying water. H_2S (about 5 mol%) present in the quench column overhead gas is rejected in the SCOT absorber when it comes into contact with the lean solvent regenerated from the AGE section. Finally, the produced off-gas containing a small amount of H_2S (<50 ppm) goes to an incinerator, and the resulting Claus flue gas (about 70 mol% of CO_2) is directly discharged into the atmosphere.

To prevent hydrate formation and corrosion, the entrained water in the sweet gas must be reduced to less than 0.1 ppm by dehydration.[38] In the gas industry, triethylene glycol (TEG) is the most common liquid desiccant as it exhibits high absorption efficiency and a high boiling point.[39] An enhanced TEG dehydration process shown in Fig. 6(c) is employed. In this process, the sweet gas flows into a TEG contactor where it is counter-currently contracted and dried by a rich TEG solvent. The enriched TEG solvent leaving the contactor bottom flows

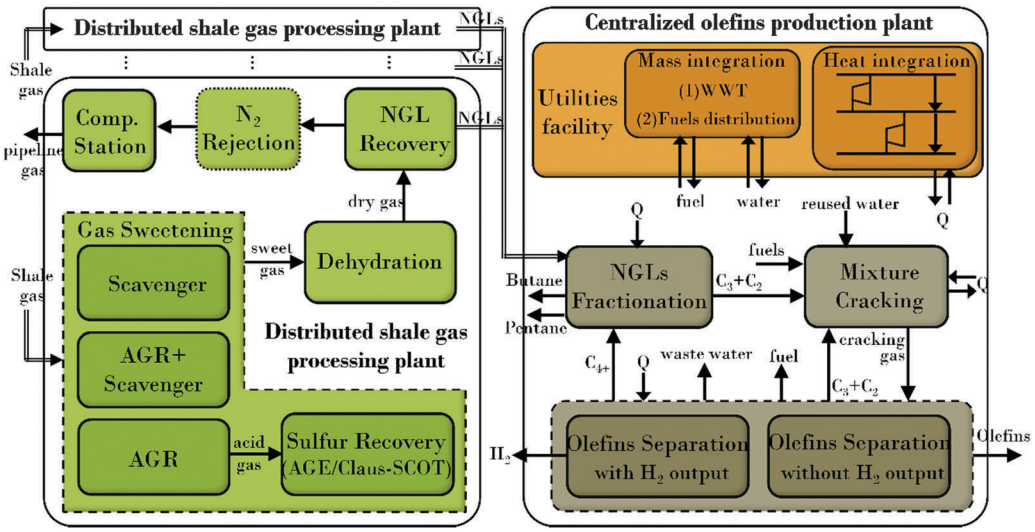

Fig. 5 Process superstructure of the proposed distributed-centralized model.

through a TEG till to regenerate the solvent. To further strip off water from the TEG solvent, a modified surge tank is employed by using a small fraction of dry gas (<0.1%) as stripping gas. This reduces the vapor partial pressure of water and thus lowers the water concentration in the lean TEG stream from 1.0–5.0 wt% to less than 0.3 wt%. The remaining dry gas exiting the contactor top is sent to the NGL recovery unit where we use cryogenic separation to partially liquefy the dry gas. This process unit uses a turbo-expansion configuration combined with an external refrigerant designed to recover about 80% of the ethane and 99.9% of the methane from the dry gas. As shown in Fig. 6d, a demethanizer is modeled as a re-boiled absorber where the non-reflux top stream (mainly containing methane) is cooled down and compressed as pipeline gas or sent to a nitrogen rejection unit depending on the nitrogen concentration; otherwise, high nitrogen content (>4 mol%) would make the heating value of the pipeline gas lower than specified. The nitrogen rejection process employs a cryogenic distillation unit integrated with a closed-loop heat pump system shown in Fig. 6(e). The re-boiler and condenser duties of the nitrogen rejecter are completely sustained by the heat pump system. Using the proposed process, more than half of the nitrogen is removed from the incoming gas while about 97.5 mol% of hydrocarbon are recovered.

3.1.2 Centralized olefin production plant. In Fig. 7(a), heavier fractions (butanes and pentanes) included in NGLs are first extracted as marketable products by sequentially passing through a depropanizer and a debutanizer. The depropanizer overhead stream, together with the ethane and propane recovered from the olefin separation unit, is sent to the mixture cracking unit as shown in Fig. 7(b). In industry, the cracking facility installation mainly includes a preheating/mixing zone and a reactor zone.[40] In the first zone, the hydrocarbon mixture is diluted with medium pressure (MP) steam to 0.4 kg kg^{-1}, and preheated to reaction temperature. The MP steam reduces the partial pressure of the hydrocarbons in the gas phase and reduces the formation of coke.[41] After that, the mixture goes into the reactor zone which includes convection, radiation and cross-over sections where the molecules of ethane and propane are broken up to generate cracking gas which includes ethylene, propylene, hydrogen, methane, acetylene, *etc.* Note that in practice the cracker is highly coupled with a fired furnace, and the heat required for cracking is provided by radiation burners located in the side walls of the furnace. The steam cracker is simulated using a three-stage Plug Flow Reactor (PFR) model.[42] The details of reactor geometry, operating conditions, reaction, and capacity are listed in Table S13 in ESI.† It is an essential factor for the overall material and energy balances to determine detailed reactions with accurate values for required kinetics and thermodynamics under the given range of conditions. According to Forment's studies,[42,43] ten independent reactions with simple rate kinetic equations are considered in this work, as given by R(1)–(10) in Table S14 in ESI.† In addition, two partial coke removal reactions are also modeled using conversion reactions. Cracking conversion is accurately simulated, as shown in Fig. S1 in ESI.† The cracker effluent can be preliminarily processed *via* multiple steps (cooling, compression, dehydration, and purification) and finally charged into the olefin separation unit.

Another depropanizer is used in the olefin separation unit to reject the heavier fractions in the cracking gas. After that, the elimination of a small amount of acetylene is implemented by a front-end hydrogenator according to reactions (9)–(10). The reactor effluent is cooled and sent to a syngas separator where about 99.9% of the syngas is rejected from the cracking gas. Note that the condenser of the syngas separator operates at extremely low temperature (−120 °C) due to the low boiling points of H_2 and CO. The rejected overhead syngas contains about 80.0 mol% H_2, 18.0 mol% CO, and other impurities (C_2H_4, CH_4, and C_2H_6). This stream can be directly considered as the furnace fuel or used for H_2 production. In the latter case, syngas is processed in a common PSA system (cold box and PSA block) for the recovery of H_2. The PSA block is modeled using a

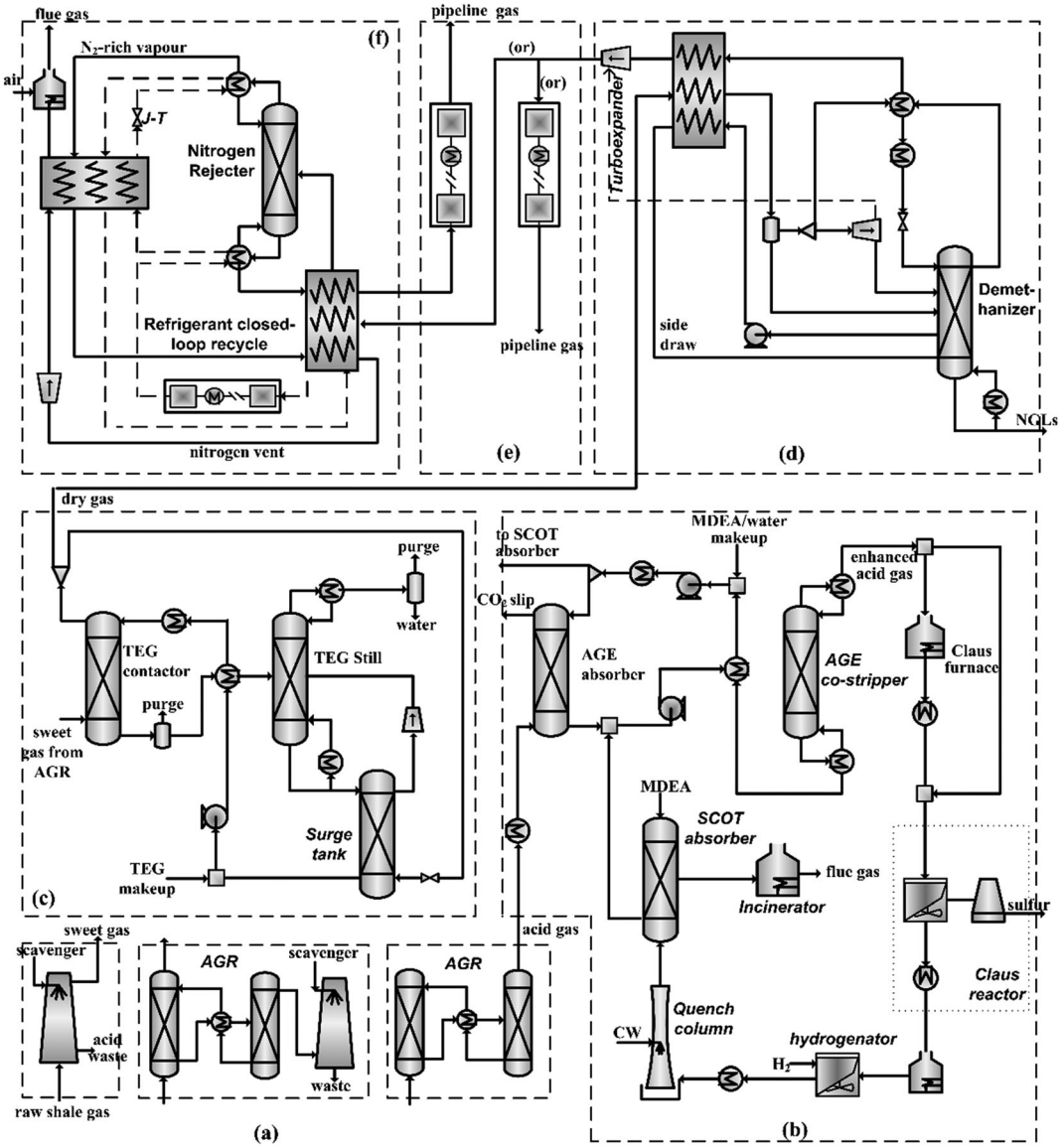

Fig. 6 Process flowsheet of the distributed shale gas processing facility. (a) Gas sweetening; (b) sulfur recovery; (c) dehydration; (d) NGL recovery; (e) the compression station; (f) N_2 rejection.

component separator that recovers 85.0% of the H_2 with 99.5 mol% purity. Pure H_2 exits the PSA block at 20 bar, and 10–15% of the H_2 is used as process H_2 to hydrogenate sulfur dioxide and acetylene. The pressure of the final H_2 product is increased to 60 bar, a pressure suited for long-range pipeline transport. Moreover, the PSA tail gas and rejected CO are used as furnace fuels.

The bottom liquid from the syngas separator is charged into a deethanizer that is designed to separate C_2 hydrocarbons from C_3 hydrocarbons. The resulting C_2 hydrocarbon stream goes to an ethylene splitter which operates at low temperatures (−25 to −75 °C) and separates the feed stream into three products: (1) an overhead product, which mainly contains small amounts of methane (<1 mol h^{-1}) and is charged to the furnace as the cracking fuel; (2) a side-draw product with 99.9 wt% polymer grade ethylene as a marketable chemical product; (3) a third product with more than 98 wt% ethane leaving the splitter bottom fed into the mixture cracking unit as the feedstock. In addition, the C_3 hydrocarbons in the bottom of the deethanizer are fed into a propylene splitter, which integrates two sub-distillation units and purifies the propylene product to the polymer grade (99.5 wt%).

3.2 Heat and mass integration

The interconnectivity of all units in the entire shale gas gas-to-olefin process has been discussed in previous sections. Heat and mass integration of the process is further carried out for the centralized olefin production plant aiming to achieve considerable saving of the utilities.[44] Fig. 8 shows the minimum energy requirements (MER) of the flowsheeting options for the centralized plants with/without H_2 production. The curves shown on the left of Fig. 8 highlight that the MER for all

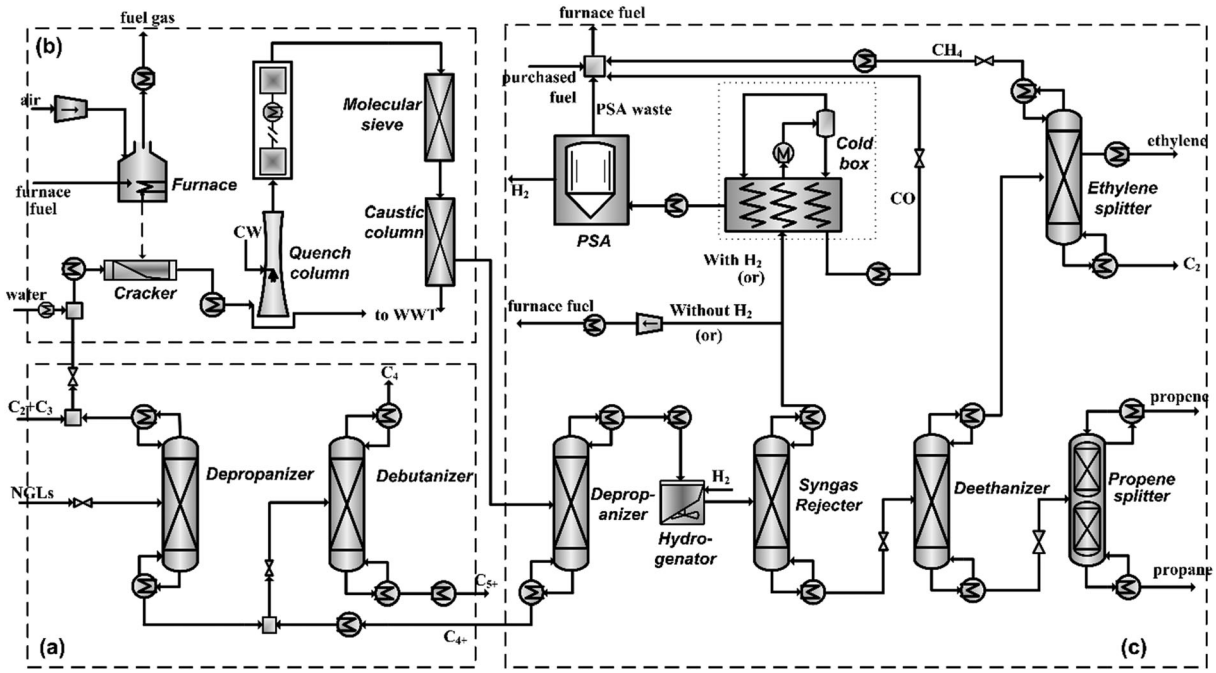

Fig. 7 The process flow diagram of a centralized olefin production plant. The utility facility is not depicted. (a) NGL fractionation; (b) mixture cracking; (c) olefin separation.

centralized plants without H_2 production are zero (see Fig. 8a and c), while the minimum consumption of the refrigerant amounts to 79–113 kW MW_{NGLs}^{-1}. If the H_2 production option is selected, we observe that a process pinch begins to appear (see Fig. 8b and d), and the MER on the hot side significantly increase from zero to 130–141 kW MW_{NGLs}^{-1}. Thus, as shown in Fig. 5 and 7, additional fuel (19–41 kW MW_{NGLs}^{-1}) from the fuel distribution system except the PSA waste is needed for the fired furnace. The difference indicates that the plant without H_2 production is more suitable for this study because it is self-sufficient in terms of energy. Furthermore, it emits much less CO_2 by using H_2-rich syngas as fired furnace fuel. Thus, we only consider the no H_2 production option in the rest of this article.

Fig. 8c also highlights the opportunity for heat recovery for power generation from the sensible heat of cracking gas, and an excess 35–50 kW MW_{NGLs}^{-1} can be recovered between 400–800 °C using the combined heat and power (CHP) technique. Once this stream is exhausted, this study uses the software SYNHEAT[45] to design the heat exchanger network among the rest of the process streams using a specialized mixed integer non-linear programming (MINLP) model. The optimized energy consumptions are listed in Table 2.

Another sub-problem is to optimize the water usage using mass integration after all water sources and sinks are identified. Similar to the studies of Gabriel *et al.*[46] and Martínez *et al.*,[47] the integration is based on a direct recycle strategy to establish targets for minimum water consumption and discharge. The direct recycle strategy is complemented by taking into account the water impurities of all potential sources and allowed water impurities of the potential sinks. This study considers that the blowdown from the quench column (Fig. 6b) contains minimal total dissolved solids (TDS), oxygenated compounds (CO and CO_2), and hydrocarbons (C_{1+}). This blowdown, along with other water sources (*e.g.*, from the CHP plant), is sent to a waste water treatment (WWT) unit mainly consisting of multi-effect distillation (MED) and TDS removal units. The MED unit normally pretreats the incoming water and reduces the oxygenated compounds and hydrocarbons to less than 10 ppm and 0.1 ppm. There are no sufficient data on the properties of process water to design a detailed post-treatment section, so the MED generated water is assumed to be directly sent to the TDS removal unit where the process water is further desalinated by the TDS removal technique according to the quality specifications[48] for cooling water and boiler feed water listed in Table S15 in ESI.†

4. Energy–water–carbon nexus and metrics

In order to better understand the energy–water–carbon nexus, Fig. 9 shows a network diagram for the STO projects that includes all potential contributions from the cradle to gate boundary. Detailed descriptions of process models have been previously provided in the above-mentioned sections. As can be seen in this figure, two allocation points (point "A") for co-products exist in the energy–water–carbon nexus, and the corresponding coefficients are f_a(ngl) and f_a(oe). The allocation method for the desired product normally includes mass-based, energy-based, and economic value-based methods.[27,49] Considering that olefins belong to chemical products, a mass-based allocation method is applied to normalize the energy and

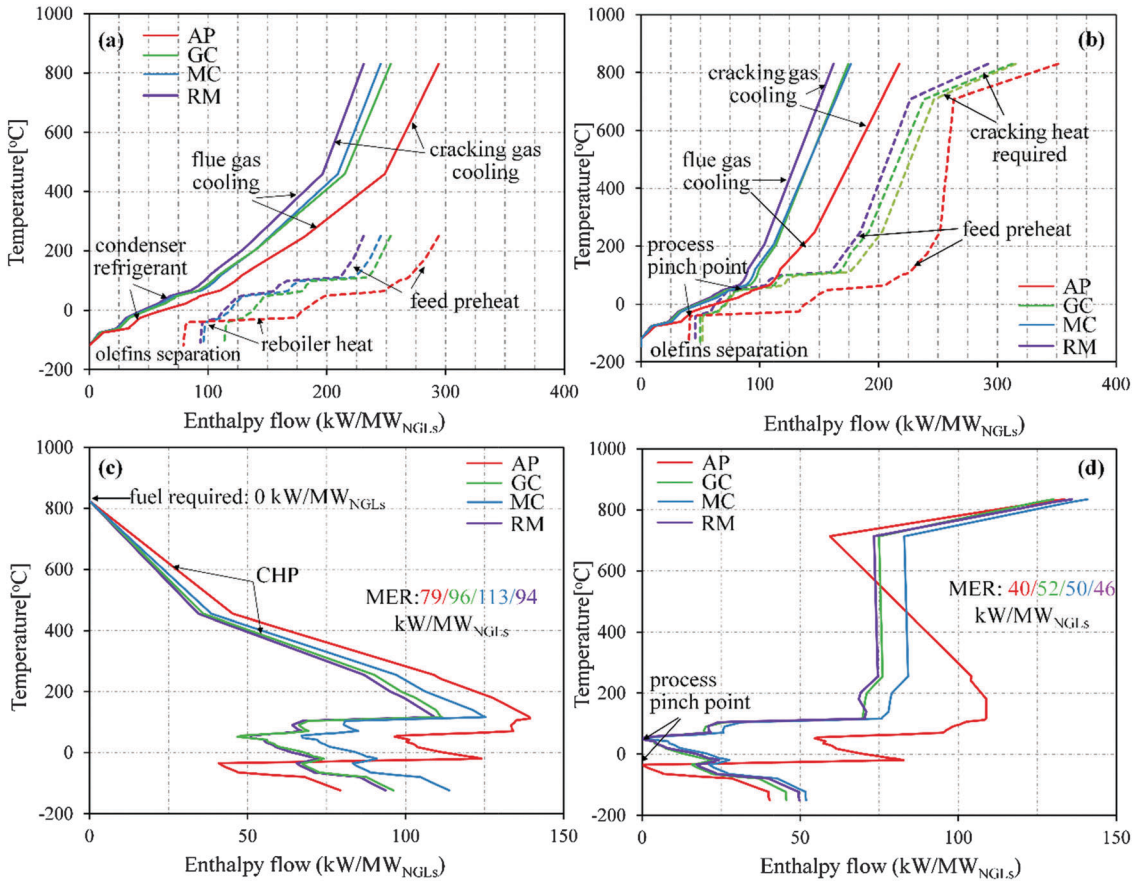

Fig. 8 Heat integration and MER on the composite/grand composite curves for the centralized olefin production plant without H_2 production (left) or with H_2 production (right).

freshwater consumptions and GHG emissions (economic value-based allocation is presented in Section 5.4). In this normalization step, the metrics are the sum of consumptions or emissions over all stages attributed to the olefins, divided by the sum of olefin production. More specifically, the metrics include life cycle energy consumption (η_{le}), the life cycle freshwater footprint (η_{lw}), and life cycle GHG emissions (η_{ghg}) in functional units of GJ per t, kg kg^{-1} and kg CO_2-eq per kg, respectively, as listed in eqn (2)–(4).

$$\eta_{le} = \left\{ \begin{array}{l} E_{SP} f_a(\mathrm{ngl}) + \left[\dot{M}_{sg} \mathrm{HHV}_{sg} - \sum_{pg,ngl} \dot{M}_i \mathrm{HHV}_i \right. \\ \left. + \left(\mathrm{heat} + \frac{\mathrm{refri}}{\mathrm{cop}} + \frac{\mathrm{electri}}{\eta_e} \right)_{GP} \right] \cdot f_a(\mathrm{ngl}) \\ + \left[\dot{M}_{ngl} \mathrm{HHV}_{ngl} - \sum_{oe,bu,pe} \dot{M}_i \mathrm{HHV}_i \right. \\ \left. + \left(\mathrm{heat} + \frac{\mathrm{refri}}{\mathrm{cop}} + \frac{\mathrm{electri}}{\eta_e} \right)_{OP} \right] \end{array} \right\} \times \frac{f_a(\mathrm{oe})}{\dot{M}_{oe}} \quad (2)$$

$$\eta_{lw} = [(W_{SP} + W_{GP}) \cdot f_a(\mathrm{ngl}) + W_{OP}] \cdot \frac{f_a(\mathrm{oe})}{\dot{M}_{oe}} \quad (3)$$

$$\eta_{ghg} = \left\{ \begin{array}{l} [\mathrm{Em}_{GP} + \mathrm{loss}_{GP} + (\mathrm{heat} \cdot \theta_h + \mathrm{refri} \cdot \theta_r + \mathrm{electri} \cdot \theta_e \\ + W \cdot \theta_w)_{GP}] \cdot f_a(\mathrm{ngl}) + [\mathrm{loss}_{OP} + (\mathrm{heat} \cdot \theta_h + \mathrm{refri} \cdot \theta_r \\ + \mathrm{electri} \cdot \theta_e + W \cdot \theta_w)_{OP}] \end{array} \right\} \times \frac{f_a(\mathrm{oe})}{\dot{M}_{oe}} \quad (4)$$

where $\dot{M}_i$, E_i, W_i, and Em_i are the mass flow (kg h^{-1}), energy input (MW h), and emissions (kg CO_2-eq per h), respectively. The cop, η and θ are the coefficient of performance of a refrigeration cycle (%), the thermal efficiency of the power cycle (%), and the emission factor of process utilities (kg CO_2-eq per kW), respectively. The subscripts h, r, e, and w denote heat, refrigerant, electricity, and water, respectively. The other abbreviations in eqn (2)–(4) are marked in Fig. 9. We have provided the calculation equations of cop, as well as the values of coefficients η_e and θ, in Table S16 in ESI.†

For the evaluation of the energy–water–carbon nexus, the detailed data of energy usage, water usage, and GHG emissions of the shale gas production stage are given in Tables S17–S19 (ESI†), respectively. Note that the energy and water consumption as well as GHG emissions associated with pipeline manufacturing

Table 2 Summary of mass and energy balances for the STO processes

Regions	Appalachian	Gulf Coast	Mid-Continent	Rocky Mountain
Feedstock				
Shale gas, MMscfd	2006	600	991	556
Shale gas, GW (HHV)	25.4	8.9	13.7	8.8
Shale gas, kt per year	14 265	5451	7674	5413
Process utilities	Gas processing facility/olefin production plant			
Heat, MW	234/0	403/0	127/0	130/0
Cold, MW	27.4/36.2	15.6/54.3	20.0/63.9	16.3/53.2
Net power consumption, MW	88.7/−15.2	22.4/−6.7	41.3/−15.4	70.1/−9.1
On-site consumption	88.7/38.6	22.4/40.3	41.3/39.1	70.1/39.9
Power generation	0/53.7	0/47.0	0/54.5	0/49.0
Net water usage, kt h^{-1}	1.3/0.31	1.8/0.34	0.7/0.35	1.5/0.35
On-site consumption	12.6/2.8	17.7/2.6	7.0/2.5	14.6/2.6
Water recycled	11.3/2.5	16.0/2.3	6.3/2.2	13.2/2.3
Solvents, tone h^{-1}	0.08/0	0.12/0	0.09/0	0.06/0
Shale gas production[a]	Scenarios: (NT + 10 year LT)/(MT + 10 year LT)/(NT + 20 year LT)/(NT + 20 year LT)[b]			
Water usage, kt h^{-1}	1.36/2.19/0.68/1.10	0.14/0.24/0.07/0.12	0.35/0.58/0.18/0.29	0.17/0.27/0.08/0.14
GHG emitted, CO_2-eq	120/194/60/97	10/17/5.1/8.6	31/51/17/25	20/33/10/17
Energy usage, GW	1.3/2.2/0.67/1.1	0.10/0.16/0.05/0.08	0.28/0.47/0.14/0.23	0.31/0.52/0.16/0.26
NGLs	NGLs transported to the centralized olefin plant			
NGLs, tone h^{-1}	182	222	247	256
NGLs, GW (HHV)	2.37	2.88	3.19	3.30
Product outputs				
Pipeline gas, MMscfd	1879	438	868	436
Pipeline gas, GW (HHV)	22.8	5.4	10.7	5.3
Ethylene, kt per year	903	876	862	866
Propene, kt per year	94	135	135	143
Butane, kt per year	154	385	300	411
Pentanes, kt per year	70	253	159	292
Carbon input–output, kt per year[c]				
C_f input	10 170	3861	5668	3894
C_f in products	9983	3663	5445	3652
C_f vented (CH_4/CO_2)	187	197	221	241
C_f stored in coke (cracker)	0.95	1.33	1.41	1.44
Life cycle efficiency				
Carbon, %	98.2	94.9	96.1	93.8
Energy (η_{LCE}), GJ per t olefins	13.8–17.2	14.3–16.7	13.3–16.7	12.2–14.5

[a] The detailed information of energy usage, water usage, and GHG emissions in the stage of shale gas production is given in Tables S17–S19, respectively. [b] NT = near-term; MT = mid-term; LT = well lifetime. [c] Sympol C_f is defined as the mass flow of carbon atom (kt per year). Note that (1) C_f input denotes the total input of carbon atoms listed in Table 1. (2) C_f in products denotes the carbon converted to the product outputs listed in this table; (3) C_f vented covers all direct emissions such as CO_2 and other hydrocarbons; (4) C_f stored in coke is considered due to the char formation from propane, see R(5) in Table S11 in ESI.

and plant construction are not considered in the LCA. Besides, the calculation of GHG emissions focuses on the global warming effects caused by CO_2, CH_4, SO_2, and NO_x. These emissions are assessed on the basis of 100 year global warming potentials (GWP), that is, 25 kg CO_2-eq per kg CH_4 and 298 kg CO_2-eq per kg N_2O.[50]

5. Results and discussion

5.1 Process yield and consumption

Table 2 presents the mass and energy balances for all STO processes evaluated in this study. For all the cases considered, the processes driven by NGL-lean shale gases (*e.g.*, Appalachian shale gas) consume more raw materials, thus leading to more carbon input. This carbon flow of shale gas is split in the processing facilities where the NGL-lean shale gases produce significantly more outlet pipeline gas by using more process utilities. The main reason is that NGL-lean shale gases require more refrigerants and work to both liquefy the incoming dry gas and compress the pipeline gas. Note that, compared with the Gulf Coast shale gas, the Rocky Mountain shale gas that contains more N_2 needs an additional 2.5 times more power to remove the excess N_2, which involves an energy-intensive N_2 rejection process. In addition, desulfurization (AGE/Claus/SCOT) is also energy-intensive, thus more heat/fuel are required to remove sulfur from relatively H_2S-rich feedstocks like the Gulf Coast shale gas. The results of process utilities listed in Table 2 also indicate that the olefin production plants have been energy-optimized such that they are net exporters of surplus electricity. However, the proposed heat integration model only recovers the sensible heat of cracking gas, and a considerable quantity of low-rank heat (<300 °C, see Fig. 7) is not well-disposed

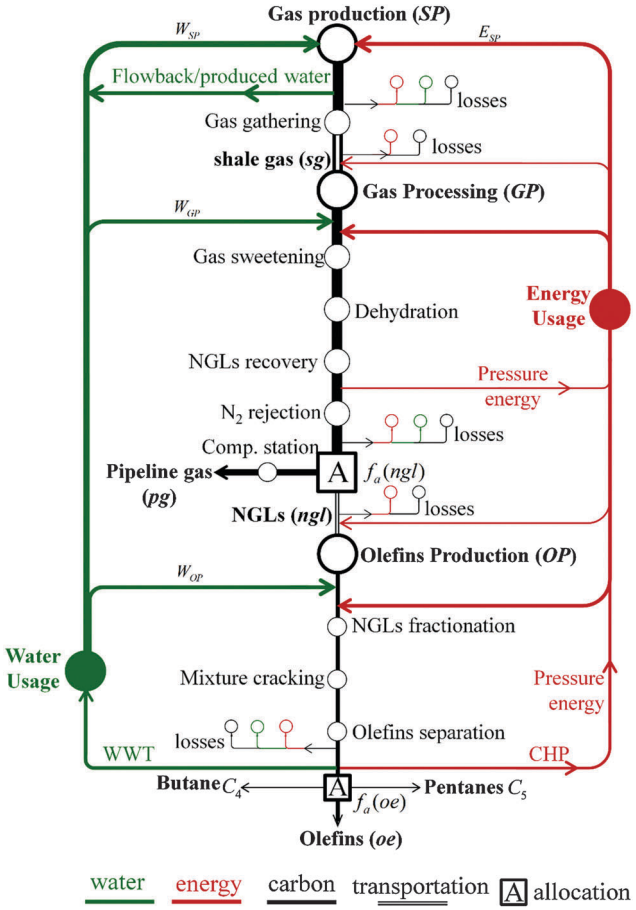

Fig. 9 Energy–water–carbon flowchart of the integrated STO projects.

due to lack of heat sinks in the olefin production plant. This challenge could be further addressed by the concept of total site heat integration[51] of the olefin production plant with the gas processing facilities or local heat sinks. To decipher the environmental footprints of shale gas production, we investigate the influences of project operating time (near-term and mid-term) and well lifetime (10 years and 20 years), resulting in four scenarios that should be considered in the normalization of energy usage, water usage, and GHG emissions, as listed in Table 2.

For the given olefin production scale, the NGLs split from the Appalachian, Gulf Coast, Mid-Continent, and Rocky Mountain shale gases are 2.37, 2.88, 3.19, and 3.30 GW (HHV), respectively. These four intermediates consume a similar amount of process utilities in the olefin plant. Considering the energy consumed in the upstream stage, the life cycle energy efficiencies of the four cases are found to be 13.8–17.2, 14.3–16.7, 13.3–16.7, and 12.2–14.5 GJ per t olefins, respectively. Besides, for the four types of shale gases considered, the carbon inputs are 10 170, 3861, 5668, and 3894 kt per year, and the corresponding carbon outputs in final products (pipeline gas, ethylene, propene *etc.*) are 9983, 3663, 5445, and 3652 kt per year, respectively. Thus, the ranking of life cycle carbon efficiency is Appalachian (98.2%) > Mid-Continent (96.1%) > Gulf Coast (94.9%) > Rocky Mountain (93.8%), indicating that NGL-rich shale gases have slightly lower carbon efficiencies by 2–5%. The reason is that the NGL-rich shale gases involve a relatively large ratio of olefin production compared with NGL-lean feedstocks, which in turn involve higher carbon losses in ethane/propane cracking.

5.2 Transportation cost and plant investment

Table 3 lists the predicted results from the distributed-centralized STO models. As indicated in this table, the number of processing facilities depends on the joint effects of feedstock quality, the NGL output of a single processing facility, and the demand of the centralized cracking plant. For example, in the near-term, producing mega-scale olefins would consume an NGL feedstock of 4375 tpd (ton per day), corresponding to a total NGL output of 20 processing facilities (100 MMscfd) located in the Appalachian region. The total number of wet wells is calculated by multiplying the wet well density (wet well/gathering system, *n*/*n*) by the number of processing facilities. For a given processing facility capacity (100 MMscfd), in the near-term, the model requires 6040, 432, 1300, and 1375 wet wells in the Appalachian, Gulf Coast, Mid-Continent, and Rocky Mountain regions, respectively. However, in the mid-term, these figures increase by 1.6–1.7 times to 9720, 732, 2160, and 2288, respectively. As mentioned above, this result is due to the declining characteristics of gas production, so the model needs newly developed wet wells to maintain mega-scale capacity. In addition, from a supply chain standpoint, the average area of the gathering system and average distances to the processing facility and centralized olefin production plant also increase accordingly. This incurs higher transportation costs for the shale gas gathering system and the NGL gathering system.

Fig. 10 shows the influences of the merging parameter and processing capacity on the unit transportation costs (total transportation cost divided by annual olefin yield) for shale gas and NGLs. As indicated in this figure, both a decrease of the merging parameter value and an increase of processing capacity lead to a decrease in the unit transportation cost. In reality, the unit transportation cost is determined by the EUR, wet well ratio, and NGL content. Among them, EUR is a main influencing factor. For instance, the Appalachian region has the lowest predicted EUR, which means that a project located in this region must be matched with the largest areas of the gathering system. An opposite example is the Gulf Coast region where, in the near-term, the unit transportation costs of shale gas and NGLs fall between \$0.14 per Mscf and \$0.41 per Mscf, and between \$0.39 per ton and \$0.16 per ton, for the given 100 MMscfd capacity of a single processing facility. Although the Rocky Mountain region produces shale gas with a relatively low EUR, the ratio of wet wells to the NGL content of this region is much better than those of others. Thus, for both shale gas and NGL transportation, the ranking of unit transportation costs is provided as follows: Appalachian > Mid-Continent > Rocky Mountain > Gulf Coast. Furthermore, as mentioned above, a plant operating in the mid-term has a larger gathering system, so it will endure about 20% more transportation costs.

The plant-level total direct cost (TDC) is estimated for each process equipment using an Aspen Capital Cost Estimator,[52]

Table 3 The predicted results from the distributed-centralized models in the Appalachian, Gulf Coast, Mid-Continent, and Rocky Mountain regions

		Near-term capacity, MMscfd				Mid-term capacity, MMscfd			
Regions	Model description	50	100	200	300	50	100	200	300
AP	Processing facilities, *n*	40	20	10	7	40	20	10	7
	Wet well/gathering system, *n*/*n*	151	302	603	862	243	487	973	1390
	Wet wellsite/gathering system, *n*/*n*	38	75	151	215	215	429	859	1226
	Gathering system area, sq. mile	62	124	247	353	100	200	399	570
	Average distance to processing facility, mile	3.61	5.11	7.22	8.63	4.58	6.49	9.17	10.96
	Average distance to centralized plant, mile	5.99	8.47	11.97	14.31	7.6	10.75	15.21	18.18
GC	Processing facilities, *n*	12	6	3	2	12	6	3	2
	Wet well/gathering system, *n*/*n*	36	71	142	213	61	121	242	364
	Wet wellsite/gathering system, *n*/*n*	9	18	36	53	15	30	61	91
	Gathering system area, sq. mile	10	19	38	57	16	32	64	97
	Average distance to processing facility, mile	1.42	2	2.82	3.46	1.85	2.61	3.69	4.52
	Average distance to centralized plant, mile	2.34	3.31	4.68	5.74	3.06	4.33	6.12	7.49
MC	Processing facilities, *n*	20	10	5	3	20	10	5	3
	Wet well/gathering system, *n*/*n*	65	130	261	434	108	215	430	717
	Wet wellsite/gathering system, *n*/*n*	16	33	65	109	27	54	108	179
	Gathering system area, sq. mile	26	52	105	174	43	86	172	287
	Average distance to processing facility, mile	2.34	3.31	4.7	6.05	3.02	4.26	6.03	7.78
	Average distance to centralized plant, mile	3.89	5.5	7.78	10.05	5	7.07	10	12.91
RM	Processing facilities, *n*	11	6	3	2	11	6	3	2
	Wet well/gathering system, *n*/*n*	125	230	460	690	208	382	764	1146
	Wet wellsite/gathering system, *n*/*n*	31	58	115	173	52	96	191	287
	Gathering system area, sq. mile	29	53	105	158	48	87	175	262
	Average distance to processing facility, mile	2.46	3.33	4.71	5.77	3.17	4.29	6.07	7.44
	Average distance to centralized plant, mile	4.08	5.52	7.81	9.57	5.26	7.12	10.07	12.33

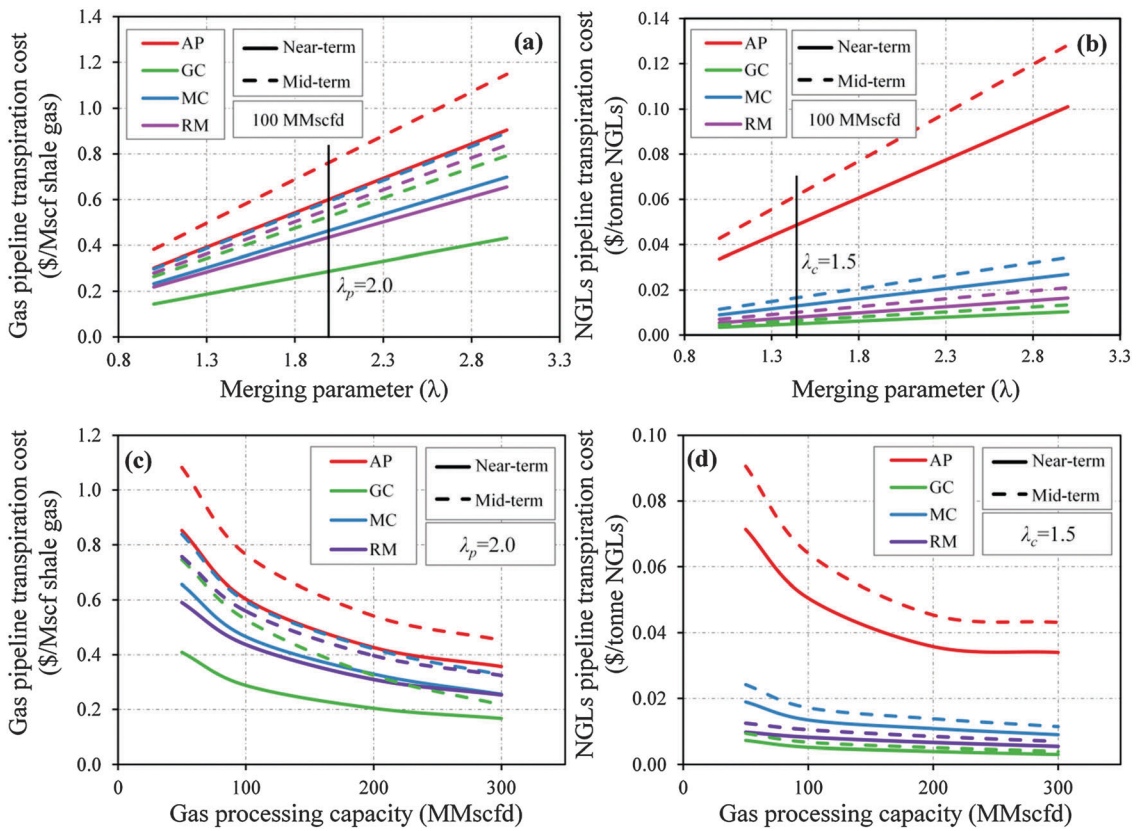

Fig. 10 Estimated costs for the transport of raw shale gas and NGLs influenced by the merging parameter and processing capacity. Detailed calculation methods of pipeline transportation costs are described in Section 1.3.3 in ESI.†

or taken from several literature sources. Detailed capital cost breakdown of each process unit is given in Table S22 in ESI.† Fig. 11(a) indicates that the processing facility investment drops with the increasing plant capacity. As listed in Table 3, the relative NGL-lean shale gases require a greater number of processing facilities (or gas gathering systems) to retain a stable NGL output shown in Table 2. This greatly increases the processing facility investment such as the project located in the Appalachian region. It is worth noting that both sulfur removal and N_2 rejection are expensive. The content of impurities affects the plant investment. An obvious example is the processing facility located in the Mid-Continent region that handles raw shale gas with relatively low H_2S and N_2 content (see Table 1) and as a result, the process has the lowest direct cost. In summary, the ranking of processing facility investment is Appalachian > Rocky Mountain > Gulf Coast > Mid-Continent. The relationship of all four STO projects located in the Appalachian, Gulf Coast, Mid-Continent, and Appalachian regions is the same in terms of the TDC, as shown in Fig. 11b. From the breakdown of TDC shown in this figure, the direct cost comes from the ten processing units. For all cases considered, the direct cost is mostly dominated by the mixture cracking unit, which makes up 55–65% of the total cost. For a given processing facility capacity (100 MMscfd), the unit capital costs of olefin production are \$1.11 per annual kg olefins, \$0.97 per annual kg olefins, \$0.94 per annual kg olefins, \$0.97 per annual kg olefins in the Appalachian, Gulf Coast, Mid-Continent, and Rocky Mountain regions, respectively.

5.3 Environmental impacts

Fig. 11 provides the breakdown of the environmental impacts of an STO project located in the Appalachian region. In a vertical comparison, the calculated metrics for the same well lifetime (10 and 20 years) but at different project operating times (near-term and mid-term) are presented. Overall, we observe 11–24%, 10–18%, and 8–14% increases of η_{le}, η_{lw}, and η_{ghg} from the near-term to mid-term, respectively. In a horizontal comparison, the η_{le}, η_{lw}, and η_{ghg} decrease 4–14%, 14–20%, 12–16% from a 10 year well lifetime to a 20 year well lifetime. In addition, the environmental impact breakdown of the projects located in other regions is listed in Table 4.

For the same shale gas feedstock, neither the project operating time nor well lifetime changes the process utility consumption nor energy losses (see Table 3). These parameters change the aggregated energy consumed in the upstream stage of gas production (pad preparation, hydraulic, well drilling, and completion[53]). For a given energy consumption per well, more wet wells (*e.g.*, in the mid-term) and a shorter well lifetime (*e.g.*, 10 years) lead to a higher fraction of energy consumption in this stage, especially for the Appalachian region (28.8%) and Rocky Mountain region (20.2%), see Table 4 for details. Overall, the ranking of η_{le} is as follows: Rocky Mountain < Mid-Continent < Gulf Coast < Appalachian. Though it requires the least numbers of wet wells, the project located in the Gulf Coast region has a higher η_{le} than those in the Rocky Mountain and Mid-Continent regions due to high process utilities consumed and high allocating factors (f_a(ngl) = 0.41; f_a(oe) = 0.61). Note that in the olefin production stage if the process energy is allocated to olefins only (f_a(oe) = 1), the specific energy consumption (SEC) ranges from 13–17 GJ per t, which is close to a traditional steam cracking facility which normally consumes 16.0–19.0 GJ for unit olefin production.[54]

Freshwater withdrawal in the upstream stage of gas production is an issue with increasing concerns. The results show that its contribution greatly changes from 2.4% water withdrawal in the Gulf Coast region to 31.0% water withdrawal in the Appalachian region. However, downstream stages of gas processing and olefin production are more important contributors to η_{lw}, as they in total represent 67–97% of the total withdrawal. In particular, for the NGL-rich shale gases, the gas processing stage becomes the most influential contributor, leading up to 62.8–66.5% water withdrawal for the Gulf Coast shale gas and 58.0–62.3% water withdrawal for the Rocky Mountain shale gas. The main reason is that high allocating factors (f_a(ngl) = 0.41 and 0.43) significantly increase the contribution of NGLs, which are further used as feedstocks to produce olefins, though NGL-rich shale gases have relatively small water cooling systems in the gas compression station. By comparison, significantly less water can be withdrawn for the Mid-Continent shale gas due to the joint effects of the allocating factor (f_a(ngl) = 0.24 and f_a(oe) = 0.68), wet well ratio (0.382, see Fig. 3b and Table S2 in ESI†), and freshwater

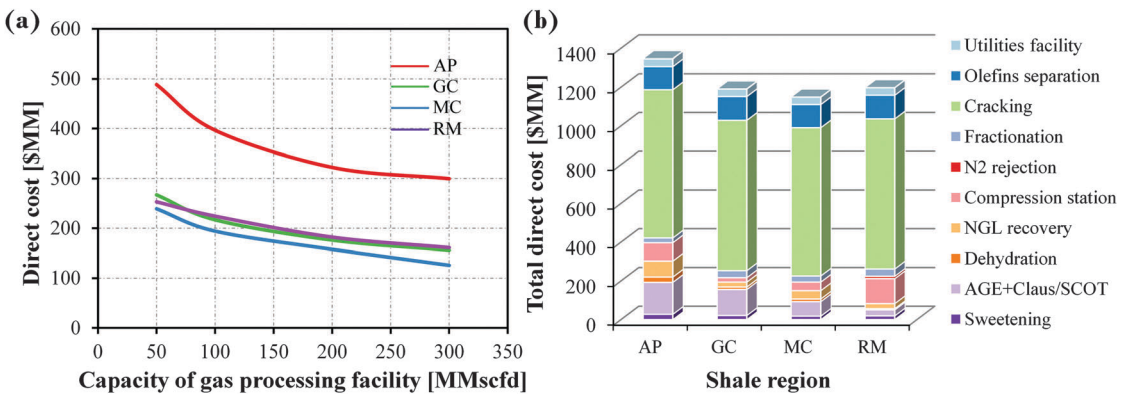

Fig. 11 Total direct cost distribution among the optimal designs. (a) Direct cost of the gas processing facility; (b) breakdown of the TDC when the capacity of the gas processing facility is 100 MMscfd.

Table 4 Environmental footprint breakdown of STO projects in Gulf Coast, Mid-Continent, and Rocky Mountain regions

Shale regions	Gulf Coast				Mid-Continent				Rocky Mountain			
Scenarios	NT + 10 year LT	MT + 10 year LT	NT + 20 year LT	NT + 20 year LT	NT + 10 year LT	MT + 10 year LT	NT + 20 year LT	NT + 20 year LT	NT + 10 year LT	MT + 10 year LT	NT + 20 year LT	NT + 20 year LT
Life cycle energy consumption (η_{le})												
Gas production, %	4.30	7.10	3.50	3.70	9.20	7.10	6.90	7.70	13.2	20.2	11.4	11.2
Gas processing, %	25.7	24.9	25.9	25.8	11.4	24.9	11.7	11.6	34.7	31.9	35.4	35.5
Olefin production, %	70.0	68.0	70.6	70.5	79.4	68.0	81.4	80.7	52.1	47.9	53.2	53.3
Total, GJ per t	14.6	14.3	15.1	14.5	13.9	14.7	13.3	13.7	13.2	14.5	12.2	12.9
Life cycle freshwater footprint (η_{lw})												
Gas production, %	4.70	7.80	2.40	4.10	13.5	20.5	7.2	11.4	6.2	9.9	3.20	5.20
Gas processing, %	64.9	62.8	66.5	65.4	28.5	26.2	30.6	29.2	60.4	58.0	62.3	61.1
Olefin production, %	30.4	29.4	31.1	30.6	58.0	53.3	62.2	59.4	33.4	32.1	34.5	33.7
Total, kg kg^{-1}	5.47	5.65	5.34	5.43	3.27	3.56	3.05	3.19	4.83	5.03	4.68	4.78
Life cycle GHG emissions (η_{ghg})												
Gas production, %	7.20	10.6	3.35	5.58	17.4	9.50	8.99	14.7	16.1	24.2	8.80	11.9
Gas processing, %	39.9	38.5	41.6	40.6	9.60	10.5	10.6	9.90	20.9	18.9	22.7	21.5
Olefin production, %	52.9	50.9	55.0	53.7	72.7	79.6	50.3	75.0	62.9	56.8	68.5	64.7
Gathering pipeline, %	0.10	0.06	0.05	0.07	0.30	0.40	0.35	0.40	0.05	0.05	0.05	0.06
Total, kg CO_2-eq per kg	1.04	1.09	1.00	1.03	0.88	0.95	0.80	0.85	0.82	0.91	0.75	0.80

withdrawal per well (5.389 MMgallon, see Table S17 in ESI†). For all cases considered in the olefin production stage, the consumption rates of freshwater are stable (about 0.34 kg h^{-1}). Thus, depending on the allocating factor, the resulting water footprints in this stage range from approximately 1.60 to 2.02 kg kg^{-1}. Overall, the freshwater consumed for the STO projects in the Appalachian, Gulf Coast, Mid-Continent, and Rocky Mountain regions ranges from 3.31–4.28 kg kg^{-1}, 5.34–5.65 kg kg^{-1}, 3.05–3.56 kg kg^{-1}, and 4.68–5.03 kg kg^{-1}, respectively.

In this study, GHG emissions from transportation pipelines are also assessed, though they account for a very small proportion (<0.5%). Similar to water withdrawal, for a given shale region, the GHG emissions seem to be sensitive to changes in project operating time and well lifetime. Another similarity exists in the shale gas production stage; the GHG emissions per kg of olefins vary from 3.70% to 31.0% of the total emissions from region to region. The olefin production stage contributes to the largest proportion (normally more than 50% of the total). This result is because of a considerable quantity of direct CO_2 emitted from the fire furnace, as well as the indirect CO_2 emissions caused by both energy loss and coke formation of the cracking reactor. Furthermore, the impurity content influences the GHG emissions in the stage of gas processing. As can be seen in Table 4, the share of gas processing in the GHG emissions could be increased significantly to around 40% in the Gulf Coast region, due to high contents of CO_2/H_2S. Nonetheless, the Appalachian shale gas containing low impurities still leads to the highest GHG emissions, because of a high carbon footprint in the upstream stage of gas production, as well as a high allocating factor of olefins (f_a(oe) = 0.82). In summary, the ranking of η_{ghg} is as follows: Gulf Coast > Appalachian > Mid-Continent > Rocky Mountain, and the corresponding values range from 1.00–1.09, 0.83–1.17, 0.80–0.95, and 0.75–0.91 kg CO_2-eq per kg olefins, respectively.

Fig. 13a shows the comparison of life cycle GHG emissions of unit ethylene produced from different feedstocks. It is well known that ethylene produced from naphtha and NG-derived ethane currently covers more than 90% of the market share, especially in North America. The normalized GHG emissions from steam cracking of naphtha and NG-ethane amount to 1.13 and 0.84 kg CO_2-eq per kg ethylene.[25] Some developing countries like China use the coal-to-olefin pathway to produce cheaper olefins, but criticisms arise due to high GHG emissions (10 kg CO_2-eq per kg ethylene) and water footprints (>20 kg water per kg ethylene). In contrast, as a new generation biofuel, sugarcane is the most environmentally friendly feedstock for ethylene production with an average value of −2.25 kg CO_2-eq per kg ethylene, followed by corn with an average value of −1.70 kg CO_2-eq per kg ethylene.[55–58]

As shown in Fig. 13b, following a mass-based allocation method, the normalized GHG emissions of shale gas projects range from 0.82 to 1.05 kg CO_2-eq per kg ethylene. Ostensibly, this environmental impact shows that shale gas may be considered as a low-carbon feedstock, though its GHG emissions are higher than that of NG-ethane by 15% on average. However, this optimistic viewpoint would be fundamentally altered if we employ an economic value based allocation method. As shown in Fig. 13b, the normalized GHG emissions are updated to 2.13, 1.37, 1.24, and 1.19 kg CO_2-eq per kg ethylene, corresponding to 118%, 31.3%, 45.1% and 36.9% of the original values, respectively. These values clearly show that shale gas becomes a high-carbon feedstock that has a greater carbon footprint than naphtha. In addition, an NGL-lean feedstock is more sensitive to the change of the allocation method. For example, compared with the mass-based method, the economic value-based allocating factors of f_a(ngl) show about 200% increase of emissions for the Appalachian shale gas and about 100% emission increase for the Mid-Continent shale gas, leading to more GHG emissions, which are ultimately attributed to ethylene. Note that the allocation method does not change the actual environmental impacts. In fact, it changes how we interpret the environmental impacts, that is, the normalized environmental impacts. In summary, the allocation method has a significant effect on our

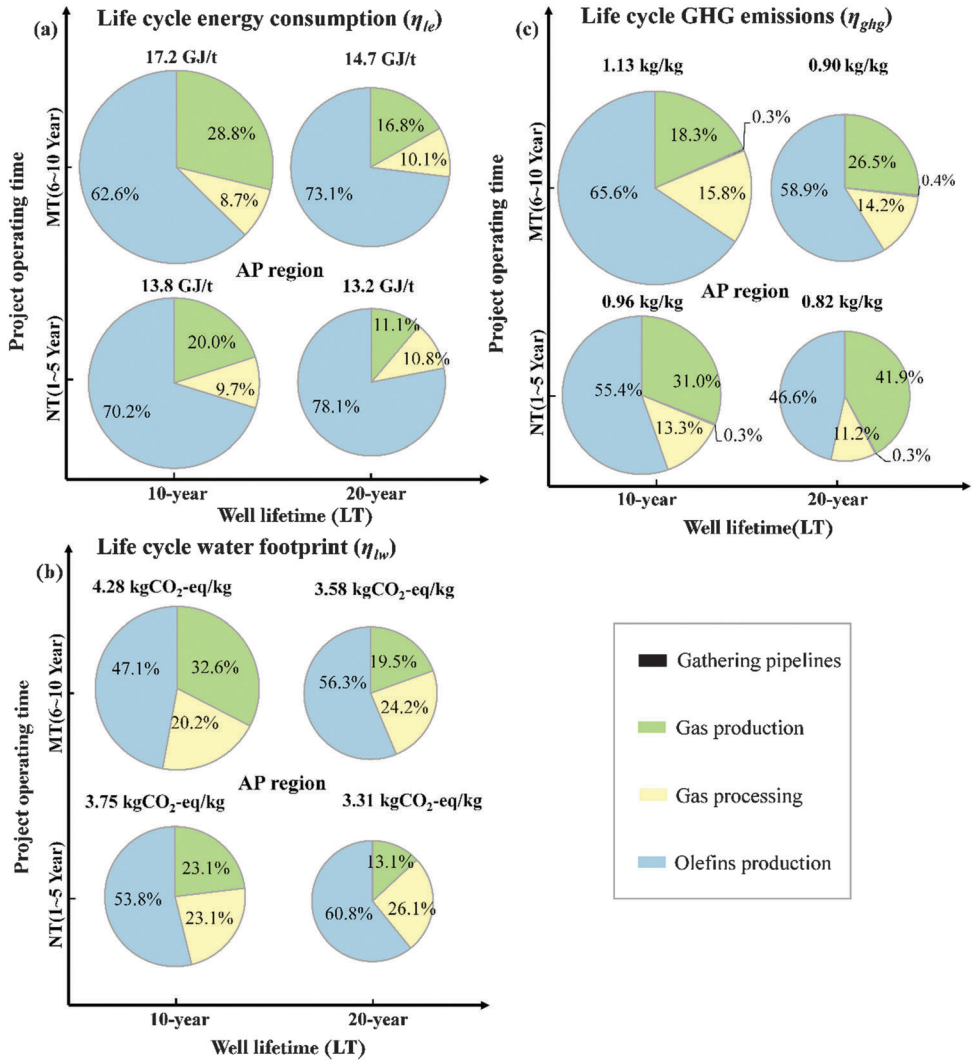

Fig. 12 Influences of well lifetime and project operating time on the environmental impacts of the STO project located in the Appalachian region. For other shale regions, the results of environmental impacts are provided in Table 4.

interpretation of the environmental impacts, especially among the two allocating points considered in the calculation.

5.4 GWP mitigation

The developing shale gas project has also resulted in growing concerns about the GHG emissions. In practice, adding a carbon capture and sequestration (CCS) operation is a key approach to reduce the process CO_2 emission, as well as the GWP.[59] A typical CCS operation mainly includes CO_2 absorption, dehydration, CO_2 compression and pipeline, as well as CO_2 injection processes.[60] In this study, the GWP mitigation opportunity comes from the implementation of CCS operation for two process streams: CO_2 clip (see Fig. 6b, in the upstream gas processing stage) and flue gas (see Fig. 7b, in the downstream olefin production stage). The CO_2 clip contains around 90 mol% CO_2 and 10 mol% H_2O, indicating that the energy-intensive CO_2 absorption process can be eliminated in the CCS operation. In contrast, the flue gas from the fired furnace contains very low CO_2 concentration (CO_2, 5.0 mol%; N_2, 92 mol%; O_2, 3.0 mol%), causing a high CCS cost. In order to better understand the cost behind CCS operation, we adopt the "CO_2 avoided cost" metric, as shown in eqn (5), to measure the incremental BESP for a year divided by the difference in unit GWP between the baseline (*i.e.* no GWP reduction) and reduction options. The results clearly show that, for the CO_2 clip, the CO_2 avoided costs of the STO projects located in Appalachian, Gulf Coast, Mid-Continent, and Rocky Mountain regions are \$30.2, \$28.6, \$31.0, and \$38.3 per kt CO_2, respectively. However, the corresponding vaules for the flue gas increase to \$100.4, \$92.2, \$91.0, and \$89.6 per kt CO_2, respectively, indicating nearly triple growths. On the other hand, the CCS operation for the flue gas has a more significant effect on reducing the life cycle GHG emissions of the STO project. Specifically, compared with the original values listed in Table 4, the metric η_{GHG} decreases by around 3.0% and 30% for the CO_2 clip and flue gas, respectively, as the CCS operation is included. This phenomenon is due to the following two reasons: (1) the CCS operation of flue gas involves a higher plant capacity; (2) the allocation factor of the olefin production stage is much

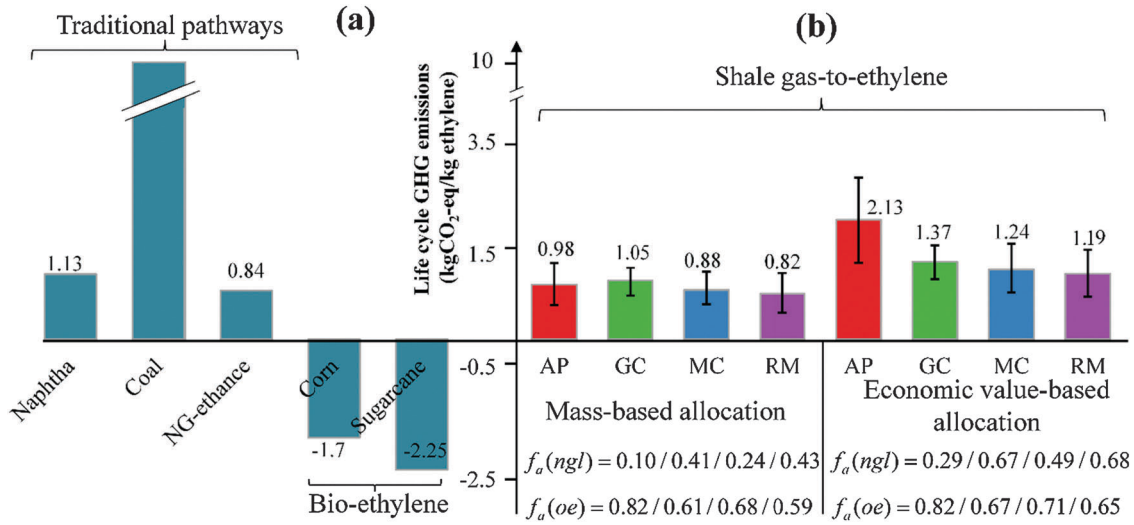

Fig. 13 Environmental impact analyses of ethylene produced from shale gas and competitors. The upper and lower error bars located on the columns in the left figure represent the values estimated under the MT + 10 year LT and NT + 20 year LT scenarios (see Table 4 and Fig. 11).

greater than that of the gas processing stage, see $f_{a(ngl)}$ and $f_{a(oe)}$ listed in Fig. 13b. Thus, a large-scale GWP mitigation of the investigated STO project would involve an expensive CCS operation of the flue gas (Table 5).

$$\text{Cost of } CO_2 \text{ avoided (\$ per kton)} = \frac{(\text{BESP})_{\text{reduction}} - (\text{BESP})_{\text{baseline}}}{(\text{GWP})_{\text{baseline}} - (\text{GWP})_{\text{reduction}}} \quad (5)$$

5.5 Economic analyses

This study investigates the economics of mega-scale STO projects. For the given EUR and raw shale gas compositions, as shown in Fig. 14, the cumulative capacities of ethylene production are 3.6, 20.4, 90.7, and 206 Mt per year for the projects located in the Appalachian, Mid-Continent, Gulf Coast, and Rocky Mountain regions, respectively. Currently, the capacity of ethylene production in the United States is about 25 Mt per year according to the EIA database.[9] Thus, the four shale regions in total would supply feedstocks for U.S. ethylene production for at least 130 years. On the other hand, the economic viability and feasibility of the STO projects are not as optimistic as the feedstock production projects. As listed in Table 1, the BGSP ranges from \$4 per MMbtu to \$9 per MMbtu, making all shale regions investigated unprofitable for the development of standalone pipeline gas projects at the current NG prices (generally less than \$4 per MMbtu[9]).

This study investigates the STO projects that integrate gas production and processing facilities to boost economic performance. A discounted cash flow economic model is used to estimate a breakeven ethylene selling price (BESP, the minimum price at which the ethylene must be sold) in terms of \$ per t. The solid marker with error bar in Fig. 14 represents the results of a Monte Carlo simulation (see Section 4 in ESI,† for detail) corresponding to a particular shale region. Overall, the predicted BESP for each region is: Mid-Continent (\$255 per t) < Gulf Coast (\$668 per t) < Rocky Mountain (\$1055 per t) < Appalachian (\$1120 per t), indicating that the BESP is highly related to the feedstock cost, as shown in Table 1. Note that only the Mid-Continent and Gulf Coast shale gases have price advantages over the current selling price and production costs of ethylene (about \$800 per t in 2012[62]). Relatively high BESPs in the Rocky Mountain and Appalachian regions for ethylene production compared to production from other sources (naphtha, NG-ethane, coal, *etc.*) potentially lead to severe economic risks for the development of shale gas-to-olefins projects. In particular, the global ethylene price is experiencing a cyclical downturn (less than \$900 per t) due to the recent collapse of oil prices, as shown in Fig. 14.

5.6 Sensitivity analyses

Table 6 summaries all influencing factors including upstream environmental footprints (energy, fresh water and emissions),

Table 5 CO_2 capacity and avoided cost

	CO_2 capacity (kton per year)				CO_2 avoided cost (\$ per kton)				η_{GHG} (kg CO_2-eq per kg olefins)			
Stream	AP	GC	MC	RM	AP	GC	MC	RM	AP	GC	MC	RM
CO_2 clip[a]	205	390	150	49	30.2	28.6	31.0	38.3	0.80–1.11	0.90–0.99	0.78–0.95	0.74–0.90
Flue gas[b]	379	609	596	642	100.4	92.2	91.0	89.6	0.51–0.82	0.73–0.82	0.51–0.68	0.50–0.65

[a] CO_2 capacity denotes the total amount of CO_2 emission in the CO_2 clip emitting from all distributed gas processing plants. [b] The most widely studied absorption process with monoethanolamine (MEA) as a solvent[61] is employed in the CCS operation.

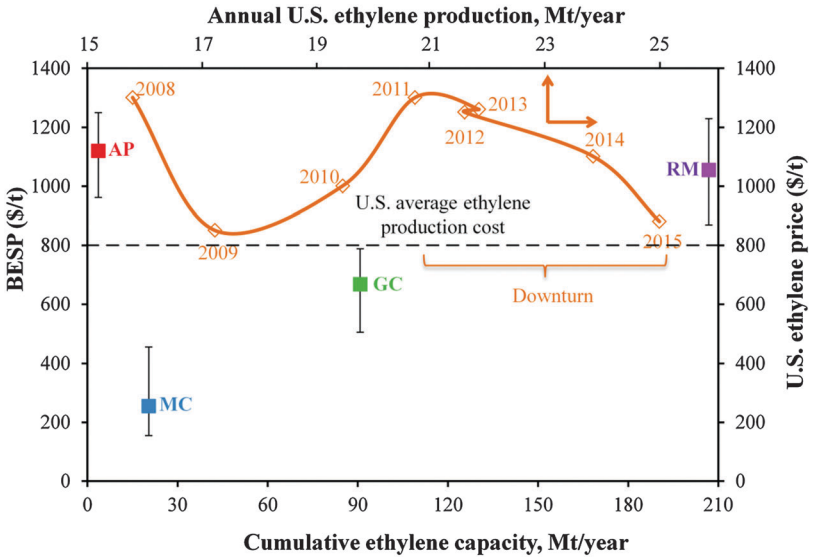

Fig. 14 Economic analyses of ethylene produced from shale gas and other competitors. The economic parameters (*e.g.*, product and feedstock prices) are provided in Table S12 in ESI,† and the detailed calculation method of BESP can be found in our previous studies.[10,11] U.S. ethylene production cost is taken from the PwC report (2012);[62] the historical ethylene prices and production (includes ethane-derived ethylene and oil-derived ethylene) are taken from the EIA database.[9]

Table 6 Summary of the major influencing factors of the project performances[a]

Factors		Life cycle energy consumption (η_{le})	Life cycle freshwater footprint (η_{lw})	Life cycle GHG emissions (η_{ghg})	Break-even ethylene selling price (BESP)
Upstream footprints	↑	↑	↑	↑	—
Feedstock composition					
Impurity content	↑	↓	↓	↓	↑
NGL content	↑	↓↑	↓↑	↓↑	↓
Well lifetime/EUR	↑	↓	↓	↓	↓
Project operating time	↑	↑	↑	↑	↑
Allocation method					
From mass to economic value		↑	↑	↑	—

[a] ↑ = positive effect; ↑ = negative effect; ↓↑ = both positive and negative effects exist.

feedstock composition, well lifetime, project operating time, as well as the allocation method. Note that the influences of gas/NGL pipelines on environmental footprints are not considered in this study due to their ignorable impacts shown in Fig. 12 and Table 4. Among these uncertainties, there is no doubt that the increase of upstream energy and freshwater consumption as well as GHG emissions increases the environmental impacts. Besides, both well lifetime and project operating time have no relationship with environmental and economic metrics in the downstream stages. In fact, they significantly influence the absolute environmental footprint and production cost in the upstream gas production stage due to the production decline characteristics of the shale well. The quality of raw shale gas depends on impurities and NGL contents. There is no doubt that the impurity has negative effects on the project performances of the gas processing stage, while the effects of NGLs are much more complex. This phenomenon is because, on one hand, the increasing NGL content helps to decrease the required number of wet wells and the capacity of gas processing facilities, which improves the environmental footprints and reduces the plant capital cost. On the other hand, NGL content is related to the calculation of allocating factors. Note that in gas production and gas processing stages, the absolute water withdrawal and GHG emissions are much higher than those of the olefin production stage. High NGL content will necessitate more GHG emissions as well as more water and energy consumption in these two stages to be ultimately allocated to olefins. Therefore, this analysis delivers an important message that the content of NGLs has both positive and negative effects on the normalized environmental impacts. This conclusion further explains why the project located in the Mid-Continent region has relatively low values of η_{lw} and η_{ghg}, as listed in Table 6.

As indicated in Section 5.3, the allocation method is the most critical factor influencing the environmental footprints.

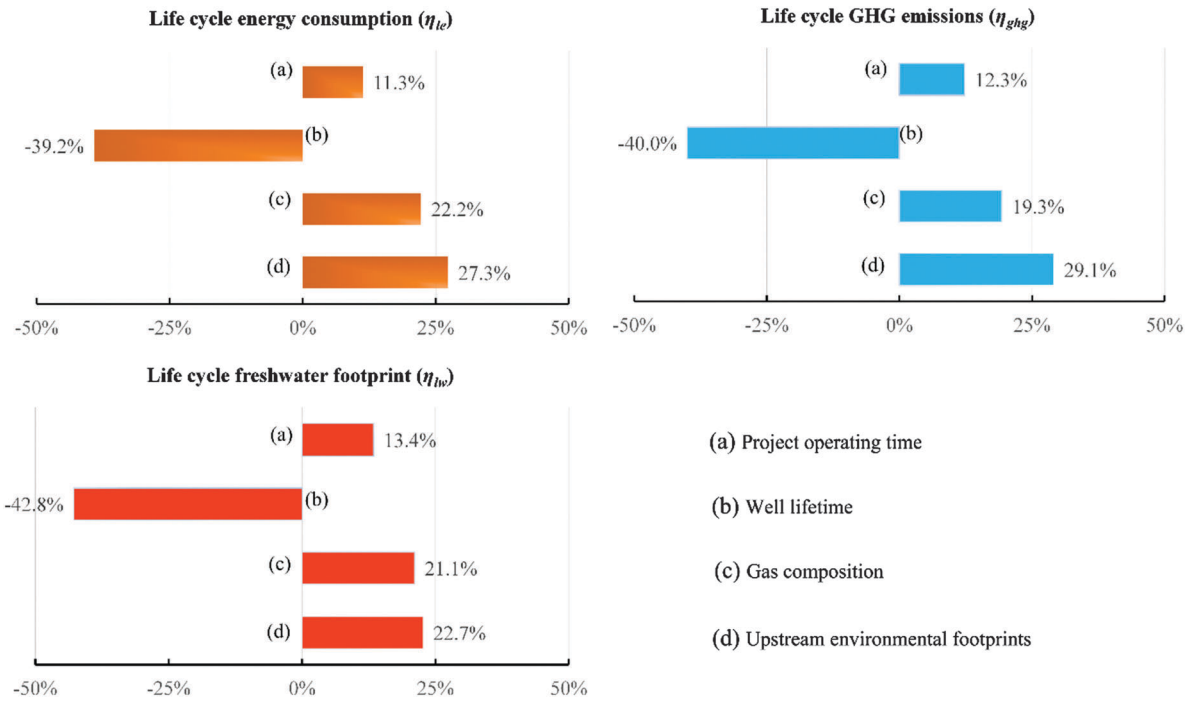

Fig. 15 Sensitivity analysis for the environmental metrics η_{le}, η_{lw}, and η_{ghg}. This analysis is based on the mega-scale STO project located in the Appalachian region, and follows a mass-based allocation method. Table S12 in ESI,† summaries the assumption, mean, and distribution used in the Monte Carlo simulation.

It is worthwhile to explicitly determine the effects of other influencing factors in a given allocation method. We conduct a sensitivity analysis for the environmental metrics with respect to the uncertainties of upstream environmental footprints, feedstock composition, well lifetime, and project operating time. Overall, the investigated factors have a similar effect on the environmental metrics, as illustrated in Fig. 15. Remarkably, the well lifetime shows the most significant influence on the metrics η_{le}, η_{lw}, and η_{ghg} and contributes 42.5%, 39.8%, and 42.8% of the variances, respectively. Note that the negative sign in this figure indicates a negative correlation between the input and output. By contrast, the upstream environmental footprints and feedstock composition play positive roles in improving the environmental metrics, accounting for 22.7–29.1% and 19.3–22.2% of the variances, respectively. In addition, the variances in project operating time contribute to 11.3–13.4% of the uncertainty in this study. Based on the above analysis, we can conclude that a longer well lifetime would improve the environmental performance in a more significant way compared to other influencing factors.

It is worth emphasizing that the STO projects investigated in this study have a mega olefin capacity consistent with the modern ethane cracker. As the plant capacity decreases, we predict that both environmental performance and economics would drop using the proposed shale gas supply and olefin production models. In particular, a half reduction in plant capacity can increase the BESP by 15–30% depending on the location of the STO project. Moreover, the decreasing plant capacity has a less obvious effect on the environmental performance. The main reason is that the plant capacity has a well-known n-tenths rule ($n < 10$) with the production cost, while both process CO_2 emission and utility consumption normally have no direct relationship with the plant capacity.

6. Conclusions

With continuous focus on the large-scale shale gas-to-olefin project in the past few years, systematic studies on process design, techno-economic modeling, and environmental impacts can determine how and where this project should be developed, as well as the resulting economic and environmental risks. In this work, we systematically addressed the process design and modelling of the large-scale olefin production from shale gas in the near-and mid-term. This project involved 594 922 shale wells (439 454 wet wells) located in four main shale regions of the U.S.: the Appalachian, Gulf Coast, Mid-Continent, and Rocky Mountain regions. In order to estimate the numbers of required shale wells, well sites, and gathering systems, detailed supply and production network models for the multisite distributed gas processing facilities and the centralized olefin production plant were established. Next, a detailed process design, modeling, and integration methodology for the candidate technologies and options were developed. We further conducted comprehensive LCA studies to determine the environmental performances of the energy–water–carbon nexus, and compared the influences of feedstock composition, project operating time, well lifetime, and the allocation method on the environmental impacts.

The results indicated that the four shale regions would in total provide at least 130 years' worth of feedstock supply for U.S. ethylene production, but only the Mid-Continent and Gulf Coast shale gases show economic advantages based on the current average production cost of ethylene (about $750 per t). Following a mass-based allocation method, for the four shale gases evaluated, the life cycle energy consumption levels were 13.8–17.2, 14.3–16.7, 13.3–16.7, and 12.2–14.5 GJ per t olefins; the life cycle water footprints were 3.31–4.28, 5.34–5.65, 3.05–3.56, and 4.68–5.03 kg kg^{-1} olefins; and the life cycle GHG emissions were 0.83–1.17, 1.00–1.09, 0.80–0.95, and 0.75–0.91 kg CO_2-eq per kg olefins, respectively. This indicated that the STO project located in the Mid-Continent region has relatively low environmental impacts, because of the lower water, energy, and carbon footprints in the upstream stage of gas production, as well as more appropriate allocating factors. Besides, the comparison of carbon footprints showed that shale gas may be still considered as a low-carbon feedstock, though its GHG emissions are still higher than those of NG-ethane by 15% on average. However, this optimistic viewpoint would be completely altered if we employed an economic value-based allocation method in which the shale gas has a greater carbon footprint than naphtha. Last, through sensitivity analysis, the well lifetime is identified as the most critical factor that significantly influences the environmental footprints.

Acknowledgements

We gratefully acknowledge financial support from the Institute for Sustainability and Energy at Northwestern University (ISEN) and from the National Science Foundation CAREER Award (CBET-1554424).

References

1 J. J. Siirola, *AIChE J.*, 2014, **60**, 810–819.
2 EIA, *Growing U.S. HGL production spurs petrochemical industry investment*, http://www.eia.gov/todayinenergy/detail.cfm?id=19771, accessed 06/16/2015.
3 EIA, *Hydrocarbon Gas Liquids (HGL): Recent Market Trends and Issues*, U.S. Energy Information Administration, Washington, DC, 2014.
4 S. F. Mitchell and D. F. Shantz, *AIChE J.*, 2015, **61**, 2374–2384.
5 J. Foster, *Can shale gale save the naphtha crackers?*, Platts, 2013.
6 Marcellus Shale gas.us, *Marcellus Shale gas well production statistics*, http://www.marcellus-shale.us/Marcellus-production.htm, accessed 06/16, 2015.
7 DrillingInfoInc, HPDI Production Database, Austin, TX, 2012.
8 D. Hughes, *Drilling Deeper: A Reality Check on U.S. Government Forecasts for a Lasting Tight Oil & Shale Gas Boom*, Post Carbon Institute, Santa Rosa, California, 2014.
9 EIA, *NATURAL GAS*, http://www.eia.gov/naturalgas/weekly/, accessed 06/20, 2015.
10 C. He and F. You, *AIChE J.*, 2015, **61**, 1209–1232.
11 C. He and F. You, *Ind. Eng. Chem. Res.*, 2014, **53**, 11442–11459.
12 C. E. Clark, R. M. Horner and C. B. Harto, *Environ. Sci. Technol.*, 2013, **47**, 11829–11836.
13 J.-P. Nicot and B. R. Scanlon, *Environ. Sci. Technol.*, 2012, **46**, 3580–3586.
14 J. Gao and F. You, *AIChE J.*, 2015, **61**, 3739–3755.
15 J. Gao and F. You, *AIChE J.*, 2015, **61**, 1184–1208.
16 L. Yang, I. E. Grossmann, M. S. Mauter and R. M. Dilmore, *AIChE J.*, 2015, **61**, 1770–1782.
17 L. Yang, I. E. Grossmann and J. Manno, *AIChE J.*, 2014, **60**, 3490–3501.
18 J. Gao and F. You, *ACS Sustainable Chem. Eng.*, 2015, **3**, 1282–1291.
19 R. W. Howarth, *Energy Sci. Eng.*, 2014, **2**, 47–60.
20 C. L. Weber and C. Clavin, *Environ. Sci. Technol.*, 2012, **46**, 5688–5695.
21 A. Brandt, G. Heath, E. Kort, F. O'Sullivan, G. Pétron, S. Jordaan, P. Tans, J. Wilcox, A. Gopstein and D. Arent, *Science*, 2014, **343**, 733–735.
22 A. Burnham, J. Han, C. E. Clark, M. Wang, J. B. Dunn and I. Palou-Rivera, *Environ. Sci. Technol.*, 2011, **46**, 619–627.
23 ArcGIS, Water Solutions Opportunities in ArcGIS database, http://www.arcgis.com/, 2015.
24 O. S. Francis and P. Sergey, *Environ. Res. Lett.*, 2012, **7**, 044030.
25 M. Ghanta, D. Fahey and B. Subramaniam, *Appl. Petrochem. Res.*, 2014, **4**, 167–179.
26 B. Vora, T. Marker, P. Barger, H. Nilsen, S. Kvisle and T. Fuglerud, *Stud. Surf. Sci. Catal.*, 1997, **107**, 87–91.
27 D. Zavala-Araiza, D. T. Allen, M. Harrison, F. C. George and G. R. Jersey, *ACS Sustainable Chem. Eng.*, 2015, **3**, 492–498.
28 EIA, *Review of Emerging Resources: U.S. Shale Gas and Shale Oil Plays*, U.S. Energy Information Administration, Energy-Washington, DC, 2011.
29 J. D. Baihly, R. M. Altman, R. Malpani and F. Luo, *Shale gas production decline trend comparison over time and basins. In SPE annual technical conference and exhibition*, Society of Petroleum Engineers, Richardson, 2010.
30 A. Berman, *After The Gold Rush: A Perspective on Future U.S. Natural Gas Supply and Price*, Vienna, Austria, 2012.
31 MIT. Shale Gas Economic Sensitivities, Boston, 2011.
32 H. Siegel, *Bakken 5-Year Drilling & Completion Trends*, 2015, http://www.dtcenergygroup.com/bakken-5-year-drilling-completion-trends/, accessed 06/02/2015.
33 S. Mokhatab and W. A. Poe, *Handbook of Natural Gas Transmission and Processing*, Gulf Professional Publishing, Boston, 2nd edn, 2012, pp. 253–290.
34 J. G. Speight, *Shale Gas Production Processes*, Gulf Professional Publishing, Boston, 2013, pp. 101–119.
35 K. Bullin and P. Krouskop, *Oil Gas J.*, 2009, **107**, 50–55.
36 L. E. Parks, D. Perry and R. Fedich, *Proceedings of the 2nd Annual Gas Processing Symposium*, Elsevier, Amsterdam, 2010, vol. 2, pp. 229–235.
37 S. Mokhatab and W. A. Poe, *Handbook of Natural Gas Transmission and Processing*, Gulf Professional Publishing, Boston, 2nd edn, 2012, pp. 291–316.

38 S. Mokhatab and W. A. Poe, *Handbook of Natural Gas Transmission and Processing*, Gulf Professional Publishing, Boston, 2nd edn, 2012, pp. 317–352.
39 A. Bahadori, *Natural Gas Processing*, Gulf Professional Publishing, Boston, 2014, pp. 441–481.
40 M. S. Yancheshmeh, S. S. Haghighi, M. Gholipour, O. Dehghani, M. Rahimpour and S. Raeissi, *Chem. Eng. J.*, 2013, **215**, 550–560.
41 M. K. Sabbe, K. M. Van Geem, M. F. Reyniers and G. B. Marin, *AIChE J.*, 2011, **57**, 482–496.
42 G. P. Froment, B. O. Van de Steene, P. S. Van Damme, S. Narayanan and A. G. Goossens, *Ind. Eng. Chem. Process Des. Dev.*, 1976, **15**, 495–504.
43 G. F. Froment, B. O. Van De Steene, P. J. Vanden Berghe and A. G. Goossens, *AIChE J.*, 1977, **23**, 93–106.
44 M. Gassner, F. Vogel, G. Heyen and F. Maréchal, *Energy Environ. Sci.*, 2011, **4**, 1726–1741.
45 T. F. Yee and I. E. Grossmann, *Comput. Chem. Eng.*, 1990, **14**, 1165–1184.
46 K. J. Gabriel, P. Linke, A. Jiménez-Gutiérrez, D. Y. Martínez, M. Noureldin and M. M. El-Halwagi, *Ind. Eng. Chem. Res.*, 2014, **53**, 7087–7102.
47 D. Y. Martínez, A. Jiménez-Gutiérrez, P. Linke, K. J. Gabriel, M. M. B. Noureldin and M. M. El-Halwagi, *ACS Sustainable Chem. Eng.*, 2014, **2**, 216–225.
48 Lenntech Water Treatment Solutions, http://www.lenntech.com/applications/process/process.htm, accessed 06/21/2015, 2015.
49 N. W. Ayer, P. H. Tyedmers, N. L. Pelletier, U. Sonesson and A. Scholz, *Int. J. Life Cycle Assess.*, 2007, **12**, 480–487.
50 S. Solomon, *Climate change 2007-the physical science basis: working group I contribution to the fourth assessment report of the IPCC*, Cambridge University Press, 2007.
51 C. W. Hu and S. Ahmad, *Comput. Chem. Eng.*, 1994, **18**, 729–742.
52 Aspen Technology, Inc., *Aspen Capital Cost Estimator V7.2*; http://www.aspentech.com, 2010.
53 Y. Chang, R. Huang, R. J. Ries and E. Masanet, *Appl. Energy*, 2014, **125**, 147–157.
54 T. Ren, M. Patel and K. Blok, *Energy*, 2006, **31**, 425–451.
55 IEA-ETSAP and IRENA, *Production of Bio-ethylene: Technology Brief*, 2013.
56 R. A. F. Alvarenga and J. Dewulf, *Renewable Energy*, 2013, **59**, 49–52.
57 GREET, Argonne National Laboratory, Oak Ridge, TN, 2012.
58 E. Center, *Ecoinvent data Swiss Centre for Life Cycle Inventories*, ETH Zurich, 2009.
59 H. J. Herzog, *Environ. Sci. Technol.*, 2001, **35**, 148–153.
60 S. Anderson and R. Newell, *General Information*, 2003, **29**, 109–142.
61 A. Raksajati, M. T. Ho and D. E. Wiley, *Ind. Eng. Chem. Res.*, 2013, **52**, 16887–16901.
62 T. Gellrich and T. Analytics, *Shale gas reshaping the US chemicals industry*, Price water house Coopers LLP, Delaware, 2012.

